

Article

Human Estrogen Receptor Alpha Antagonists, Part 3: 3-D Pharmacophore and 3-D QSAR Guided Brefeldin A Hit-To-Lead Optimization toward New Breast Cancer Suppressants

Nezrina Kurtanović¹, Nevena Tomašević¹ , Sanja Matić², Elenora Proia³ , Manuela Sabatino³ , Lorenzo Antonini³ , Milan Mladenović^{1,*} and Rino Ragno^{3,*} 

- ¹ Kragujevac Center for Computational Biochemistry, Department of Chemistry, Faculty of Science, University of Kragujevac, Radoja Domanovića 12, P.O. Box 60, 34000 Kragujevac, Serbia; nezrina.mihovic@pmf.kg.ac.rs (N.K.); nevena.stankovic@pmf.kg.ac.rs (N.T.)
- ² Institute for Informational Technologies Kragujevac, University of Kragujevac, Jovana Cvijića bb, 34000 Kragujevac, Serbia; sanjamatic@kg.ac.rs
- ³ Rome Center for Molecular Design, Department of Drug Chemistry and Technology, Faculty of Pharmacy and Medicine, Sapienza University of Rome, P.le A. Moro 5, 00185 Rome, Italy; eleonora.proia@uniroma1.it (E.P.); manuela.sabatino@uniroma1.it (M.S.); lorenzo.antonini@uniroma1.it (L.A.)
- * Correspondence: milan.mladenovic@pmf.kg.ac.rs (M.M.); rino.ragno@uniroma1.it (R.R.); Tel.: +381-34336223 (M.M.); +39-49913937 (R.R.)



Citation: Kurtanović, N.; Tomašević, N.; Matić, S.; Proia, E.; Sabatino, M.; Antonini, L.; Mladenović, M.; Ragno, R. Human Estrogen Receptor Alpha Antagonists, Part 3: 3-D Pharmacophore and 3-D QSAR Guided Brefeldin A Hit-To-Lead Optimization toward New Breast Cancer Suppressants. *Molecules* **2022**, *27*, 2823. <https://doi.org/10.3390/molecules27092823>

Academic Editors: Halil Ibrahim Ciftci, Belgin Sever and Mehlika Dilek Altıntop

Received: 15 March 2022

Accepted: 23 April 2022

Published: 28 April 2022

Publisher's Note: MDPI stays neutral with regard to jurisdictional claims in published maps and institutional affiliations.



Copyright: © 2022 by the authors. Licensee MDPI, Basel, Switzerland. This article is an open access article distributed under the terms and conditions of the Creative Commons Attribution (CC BY) license (<https://creativecommons.org/licenses/by/4.0/>).

Abstract: The estrogen receptor α (ER α) is an important biological target mediating 17 β -estradiol driven breast cancer (BC) development. Aiming to develop innovative drugs against BC, either wild-type or mutated ligand-ER α complexes were used as source data to build structure-based 3-D pharmacophore and 3-D QSAR models, afterward used as tools for the virtual screening of National Cancer Institute datasets and hit-to-lead optimization. The procedure identified Brefeldin A (BFA) as hit, then structurally optimized toward twelve new derivatives whose anticancer activity was confirmed both in vitro and in vivo. Compounds as SERMs showed picomolar to low nanomolar potencies against ER α and were then investigated as antiproliferative agents against BC cell lines, as stimulators of p53 expression, as well as BC cell cycle arrest agents. Most active leads were finally profiled upon administration to female Wistar rats with pre-induced BC, after which 3DPQ-12, 3DPQ-3, 3DPQ-9, 3DPQ-4, 3DPQ-2, and 3DPQ-1 represent potential candidates for BC therapy.

Keywords: breast cancer; estrogen receptor α ; structure-based 3-D pharmacophores; structure-based 3-D QSAR; brefeldin a derivatives synthesis; anticancer activity in vitro and in vivo

1. Introduction

Estrogen receptor α (ER α) mediates as nuclear receptor (NR) the hormonal breast cancer (BC) development [1–3], being stimulated by 17 β -estradiol (E₂); the initialization of tumor progression is regulated by either genomic direct or indirect pathway [4–11], as well as by the recruitment of transcriptional basal machinery (TBM) complex (see Supplementary Material: Introduction for further information and references). As there are no known cellular mechanisms to fully suppress BC development in vivo [1], clinical cases are treated with selective estrogen receptor modulators (SERMs, mixed agonists/antagonists of ER α), and selective ER α down-regulators (SERDs, full antagonists of ER α). Both SERMs and SERDs bind the ER α ligand-binding domain (LBD, Figure 1), inducing LBD's helix 12 (H12) induced fitting, leading to different pharmacological profiles: while SERMs, as non-steroid compounds, prevent the ER α signaling at genomic direct or genomic indirect level, SERDs, as steroid-based drugs, force the rapid downregulation and proteasomal degradation of ER α [12–17]. Herein, a simplified representation of LBD, either free or saturated with

agonists, SERM, or SERD, respectively, is depicted (Figure 1). So far FDA-approved SERMs (Figure 2) are tamoxifen (Tam, Nolvadex[®]) and toremifene (Far, Fareston[®]), i.e., the representatives of SERM I generation; raloxifene (Ral, Evista[®] (Figure 1C), namely a member of the second-generation SERM family); and nafoxidine (Naf), lasofoxifene (Las, Fablyn[®]), ospemifene (Osp, Osphena[®]), and bazadoxifene (Baz, Duavee[®]) (i.e., third-generation SERMs) [16], whereas fulvestrant (Ful, Faslodex[®]) is the only FDA-approved SERD (Glaxo SmithKline's GW-5538 [1], Figure 1D, has reached clinical trials). Yet, despite indubitable efficacy, long-term treatment with Nolvadex[®] [17] causes endometrial cancer, Evista[®] [18] has modest efficacy in advanced BCs, while other SERMs exert transitory clinical effectiveness accompanied by almost-inevitable BC resistance and relapse [19,20]. The defectiveness described encourages the investigation and development of further SERM classes.

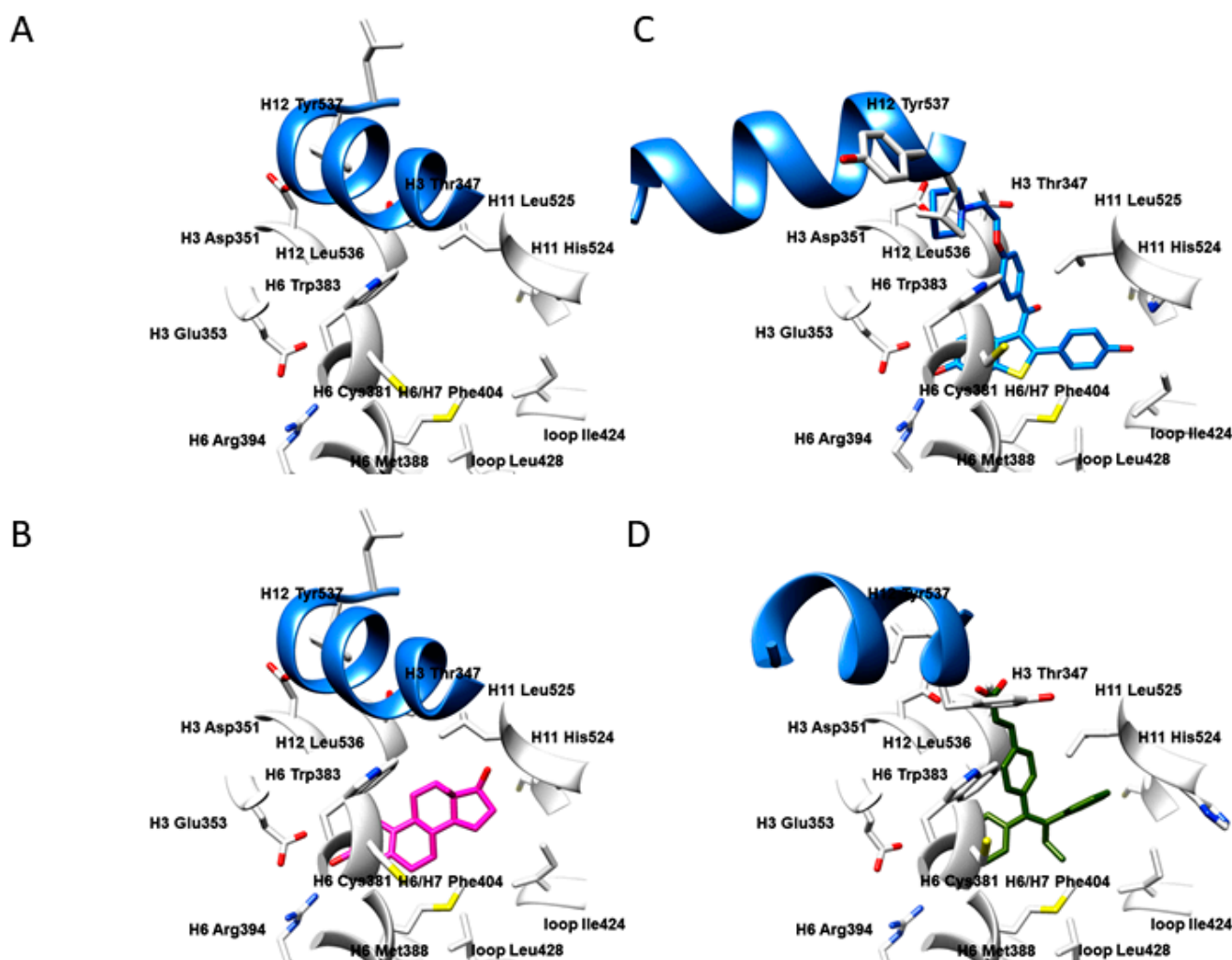


Figure 1. The active site of ER α in the apo form (PDB ID: 4Q13 [21]) (A); in complex with 17 β -estradiol (PDB ID: 1ERE [13], i.e., agonist/partial agonist) (B); in complex with Raloxifene (PDB ID: 1ERR [13], i.e., SERM antagonist) (C); in complex with GW568 (PDB ID: 1R5K [21], i.e., SERD antagonist) (D). The residues depicted as white sticks and ribbons belong to the helices H3 (residues 332–354), H6 (residues 383–394), H7 (residues 429–438), H11 (residues 517–528), H12 (residues 531–547), loop (residues 418–428), and S1 and S2 antiparallel β -sheets (residues 402–410). H12 helix is depicted as a blue ribbon, as a crucial delimiter for partial agonists, SERMs, and SERDs.

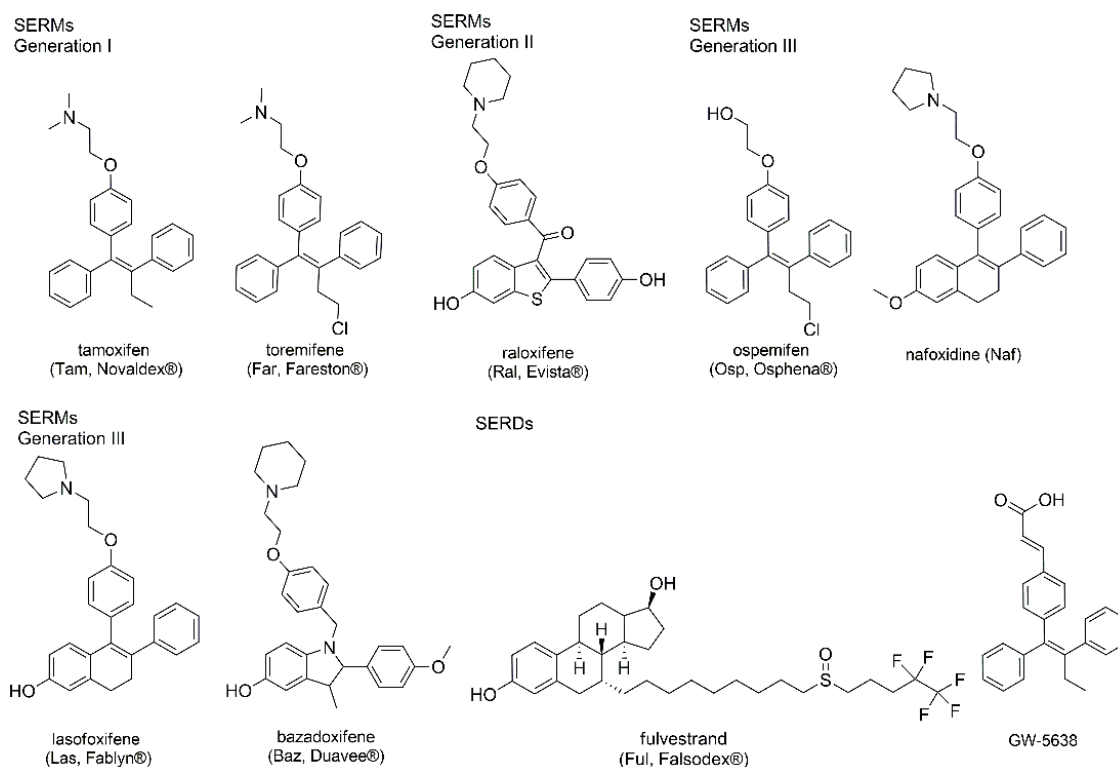


Figure 2. SERMs and SERDs as FDA-approved drugs and compounds in clinical trials for BC treatment.

Computer-aided drug design (CADD) approaches were extensively used to achieve an understanding of the potency of ER α partial agonists, SERMs, and SERDs through the development of 3-D pharmacophore hypotheses [22–58] (see Supplementary Materials: ER α 3-D pharmacophore models generation overview). Recently, a list of ER α ligands [13,59–79] was investigated to build predictive field-based SB 3-D QSAR models [80] that drove the disclosure of innovative coumarin and coumarin-like SERMs [81]. Herein (Figure 3), partial agonists, SERMs, and SERDs, co-crystallized with either wild-type (WT) or mutated (MUT) ER α s, as found deposited and available from the Protein Data Bank (39 complexes) [13,59–79], were retrieved to build structure-based (SB) 3-D pharmacophore models and atom-based 3-D QSAR models [61,62] in order to develop innovative SERMs that would exert no or diminished known side effects [17–20].

Nonetheless, to the best of the authors' knowledge, no comprehensive study has yet been conducted to explore all such structural data for generating the SB 3-D pharmacophore models that are generated herein and compared with previous ligand-based (LB) and SB findings [22–58] (see Supplementary Materials: ER α 3-D pharmacophore models generation overview). The optimal 3-D pharmacophore hypothesis and the associated 3-D QSAR model were applied in a virtual screening (VS) campaign, using the National Institute of Health database, from which Brefeldin A (BFA) was indicated as a suitable hit for hit-to-lead optimization, driving to a series of twelve new BFA derivatives with a potential of being new ER α SERM antagonists (3DPQ-1 to 3DPQ-12, Figure 3). The 3DPQ-derivatives were promptly synthesized and subjected to in vitro and in vivo biological screening. Among them, 3DPQ-12, 3DPQ-9, 3DPQ-3, 3DPQ-4, 3DPQ-2, and 3DPQ-1 showed a biological profile as a promising new SERM class of compounds for potential anticancer therapy.

2. Results and Discussion

2.1. Datasets Compilation

All the available ER α s, co-crystallized with partial agonists, SERMs, and SERDs (PDB accessed in October 2015, see Supplementary Materials: Crystal structures compilation and

preparation and Table S1, [13,59–79,82–87]) were retrieved. Unfortunately, the biological experimental data available for the bound ER α ligands (Supplementary Materials Table S1) revealed a heterogeneous distribution of the associated potencies, expressed as either pIC₅₀s ($-\log[\text{IC}_{50}]$) or pK_is ($-\log[K_i]$), and only a few of them with both values. Being higher the number of inhibitors associated with pIC₅₀s values, they were used to compile the training set (TR, Tables 1 and 2) [13,59–74]. To evaluate the under-building 3-D pharmacophore/3-D QSAR models' predictive ability, the 13 compounds, characterized by pK_is values and those with dual potencies (both pK_is and pIC₅₀s), were filed in the crystal test set (TS_{CRY}, Table 3) [69,75–79]. To indicate TR and TS_{CRY} ligands, PDB codes as listed in Tables 1–3 were used.

Furthermore, 97 known ER α binders, taken from the literature, were used to compile modeled test sets TS_{MOD1}, TS_{MOD2}, and TS_{MOD3}, grouped in agreement with the associated pIC₅₀, pK_i, and pRBA values, respectively (Supplementary Materials Tables S10–S15).

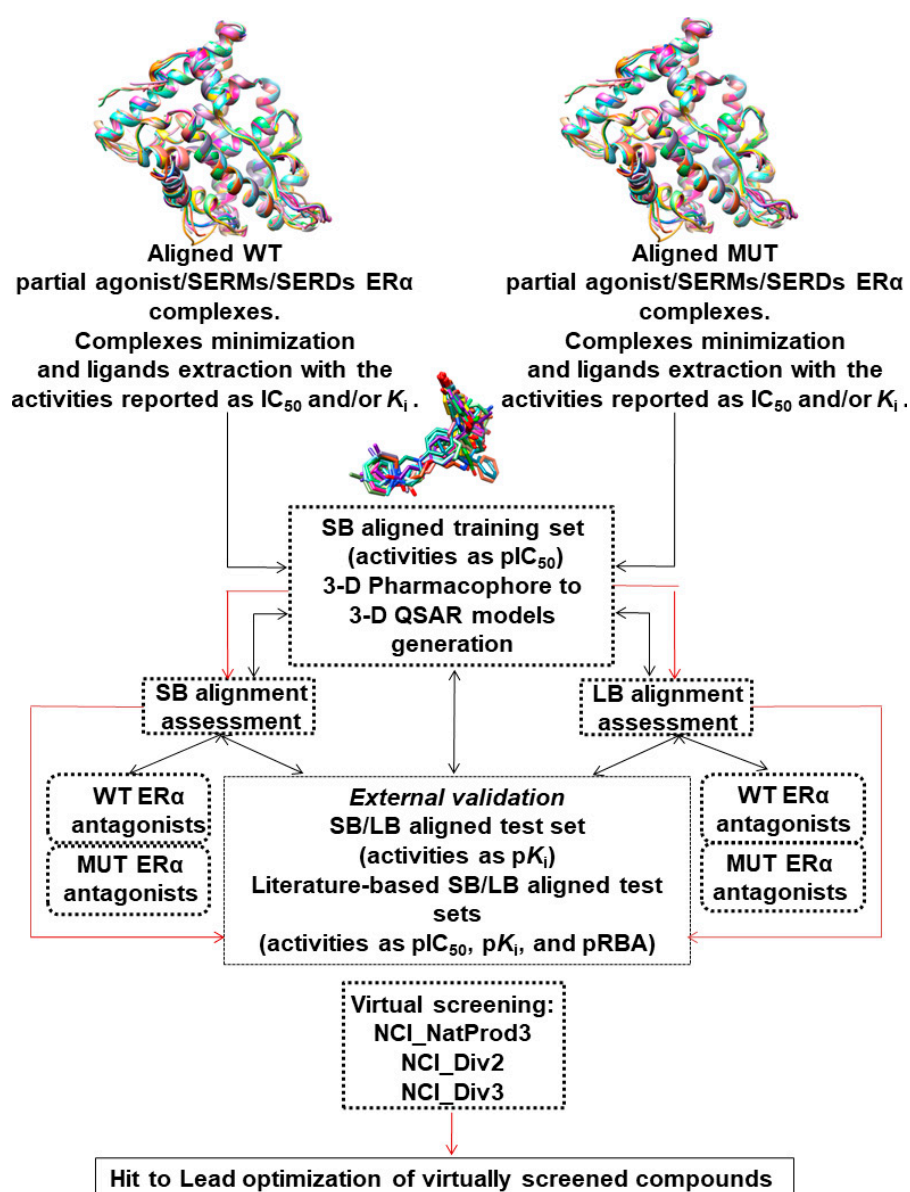
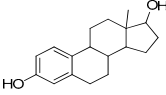
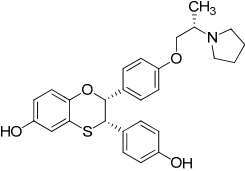
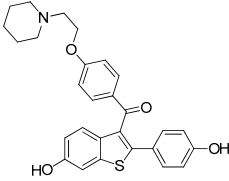
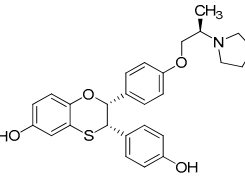
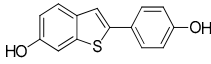
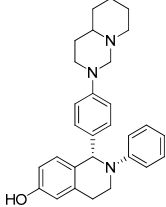
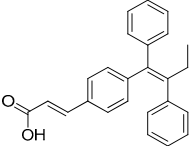
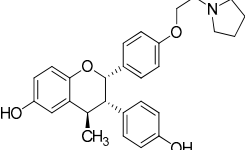
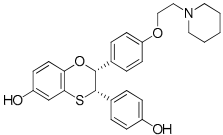
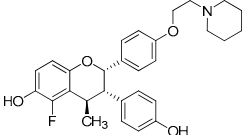
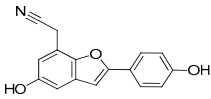
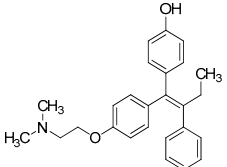
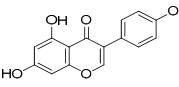
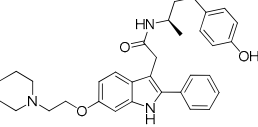
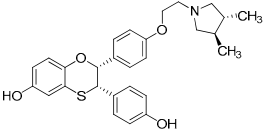
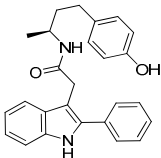
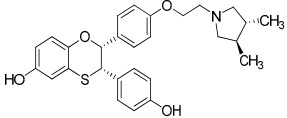
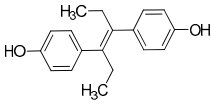


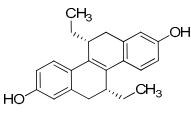
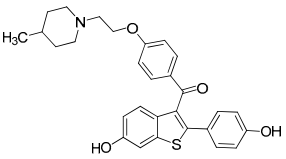
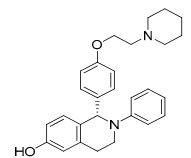
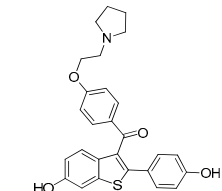
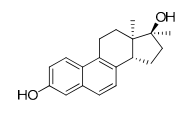
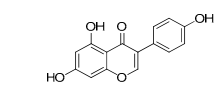
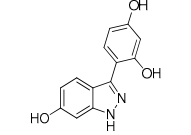
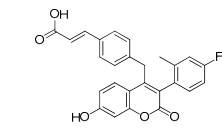
Figure 3. The overall procedure workflow used for the definition of the 3-D pharmacophore/3-D QSAR models and their analysis is depicted as a “black” pathway. The application of generated 3-D pharmacophore/3-D QSAR models in structure-based and ligand-based virtual screening is depicted as a “red” pathway.

Table 1. PDB codes, ligand structures, and pharmacological profile of wild-type (WT) estrogen receptor α complexed with antagonists and partial agonists, for the 3-D Pharmacophore hypotheses generation compounds were classified into “actives” (PDB codes marked with a star) and “inactives” (PDB codes marked with a double star) using a threshold pIC_{50} value of 7.30.

PDB	Ligand Structure	pIC_{50}	Ref.	PDB	Ligand Structure	pIC_{50}	Ref.
1ERE * PA ^a H12: CC ^b		9.24	[13]	1XP9 * SERM H12: OC		8.80	[64]
1ERR * SERM ^c H12: OC ^d		9.52	[13]	1XPC * SERM H12: OC		8.70	[64]
1GWQ ** PA H12: CC		5.85	[60]	1XQC ** SERM H12: OC		7.20	[65]
1R5K * SERD ^e H12: OC		7.40	[59]	1YIM * SERM H12: OC		8.80	[66]
1SJ0 * SERM H12: OC		9.09	[61]	1YIN * SERM H12: OC		8.80	[66]
1X7E ** PA H12: CC		5.90	[62]	2BJ4 * SERM H12: OC		8.60	[67]
1X7R * PA H12: CC		8.01	[63]	2IOG * SERM H12: OC		8.09	[68]
1XP1 * SERM H12: OC		9.30	[64]	2IOK * SERM H12: OC		9.00	[68]
1XP6 * SERM H12: OC		9.30	[64]	3ERD * PA H12: CC		9.48	[69]

^a Partial agonist; ^b H12: closed conformation; ^c SERM—mixed agonist/antagonist; ^d H12: open conformation; ^e SERD—full antagonist.

Table 2. PDB codes, ligand structures, and pharmacological profile of mutated (MUT) estrogen receptor α complexed with antagonists and partial agonists; for the 3-D pharmacophore hypothesis generation, compounds were classified into “actives” (PDB codes marked with a star *) and “inactives” (PDB codes marked with a double star **) using a threshold pIC_{50} value of 7.30.

PDB	Ligand Structure	pIC_{50}	Ref.	PDB	Ligand Structure	pIC_{50}	Ref.
1L2I * PA ^a H12: CC ^b		8.50	[2]	2R6W * SERM H12: OC		8.60	[73]
1UOM * SERM ^c H12: OC ^d		7.70	[70]	2R6Y * SERM H12: OC		8.90	[73]
2B1Z ** PA H12: CC		7.10	[71]	2QA8 * PA H12: CC		8.01	[72]
2QA6 ** PA H12: CC		7.30	[72]	5AK2 * SERD ^e H12: OC		8.40	[74]

^a Partial agonist; ^b H12: closed conformation; ^c SERM—mixed agonist/antagonist; ^d H12: open conformation; ^e SERD—full antagonist.

Table 3. PDB codes, ligand structures, and pharmacological profile of WT and MUT estrogen receptor α complexed (the qualification indicated below the code) with antagonists and partial agonists used as test set (TS_{CRY}).

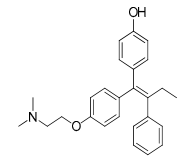
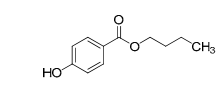
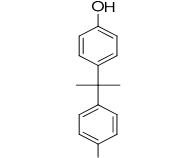
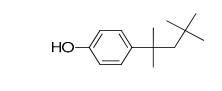
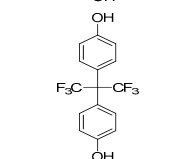
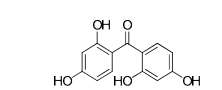
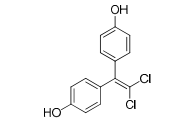
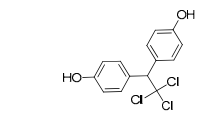
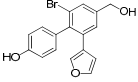
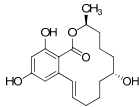
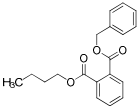
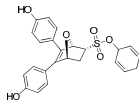
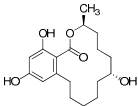
PDB	Ligand Structure	pK_i	Ref.	PDB	Ligand Structure	pK_i	Ref.
3ERT (WT) PA ^a H12: CC ^b		9.60	[69]	4MG9 (MUT) PA H12: CC		6.00	[77]
3UU7 (MUT) PA H12: CC		8.79	[75]	4MGA (MUT) PA H12: CC		6.00	[77]
3UUA (MUT) PA H12: CC		8.79	[75]	4MGC (MUT) PA H12: CC		7.00	[77]
3UUC (WT) PA H12: CC		5.70	[75]	4MGD (MUT) PA H12: CC		6.00	[77]

Table 3. Cont.

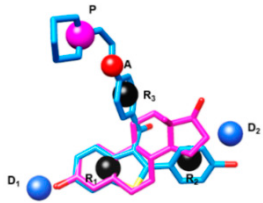
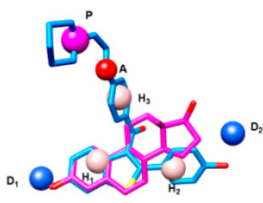
PDB	Ligand Structure	pK_i	Ref.	PDB	Ligand Structure	pK_i	Ref.
4DMA (WT) PA H12: CC		5.60	[76]	4TUZ (MUT) PA H12: CC		10.00	[78]
4MG6 (MUT) PA H12: CC		6.00	[77]	4ZN9 (MUT) PA H12: CC		9.60	[79]
4MG8 (MUT) PA H12: CC		10.00	[77]				

^a Partial agonist; ^b H12: closed conformation.

2.2. 3-D Pharmacophore and 3-D QSAR Modeling and Models' Interpretation

SB 3-D pharmacophore hypotheses (**3-D Phyp**) and atom-based **3-D QSAR** models were built with the TR using Schrödinger's PHASE program [88,89] and interpreted as a unique **3-D Phyp/3-D QSAR model** ensemble. To derive the best PHASE hypotheses (associated with the highest q^2 values [90,91]), TR molecules were classified into "actives" and "inactives," using a pIC_{50} threshold value of 7.30, as suggested by the default settings (Tables 1 and 2). While searching for the optimal **3-D Phyp/3-D QSAR model** ensemble, all the available pharmacophoric feature combinations were explored, from which both common pharmacophore hypothesis (CPH) and atom-based 3-D QSAR models were built (top hypotheses are displayed in Supplementary Material Table S2). Based on the highest associated q^2 values, the two best hypotheses were selected, **ADDHHHP.13** and **ADDRRRP.11** (Table 4, Figure 4), herein named **3-D PhypI** and **3-D PhypII**, respectively. Both hypotheses consisted of one hydrogen-bond acceptor (**A**), two hydrogen-bond donators (**D₁** and **D₂**), either three hydrophobic (**H₁**, **H₂**, and **H₃**) or aromatic rings (**R₁**, **R₂**, and **R₃**), and one with positively ionizable (**P**) features, which were coupled with the under-developing **3-D QSAR model PLS-coefficients** contour maps revealing the areas associated to positive and negative steric (**GREEN_{PLS-coefficients}** and **YELLOW_{PLS-coefficients}**) and HB bonding (**BLUE_{PLS-coefficients}** and **RED_{PLS-coefficients}**) interactions, respectively. Considering that in the PHASE definition, the **H** features are statistically more important, **3-D PhypI** was consequently taken as the base model for the upcoming discussion (Table 4). Only the most important implications of two top hypotheses (Figures 5 and S1–S9) on the potency against ER α were presented, whereas the detailed analyses and comparison with previous hypotheses [22–58] are reported as Supplementary Materials (see the sections The Origin/Significance of the **D₁** Feature and the Interrelated PLS-coefficients, The Origin/Significance of the **D₂** Feature and the Interrelated PLS-coefficients, The Origin/Significance of the **H₁/R₁** Feature and the Interrelated PLS-coefficients, The Origin/Significance of the **H₂/R₂** Feature and the Interrelated PLS-coefficients, The Origin/Significance of the **H₃/R₃** Feature and the Interrelated PLS-coefficients, The Origin/Significance of the **A** Feature and the Interrelated PLS-coefficients, and The Origin/Significance of the **P** Feature and the Interrelated PLS-coefficients). For the graphical analysis [80,92,93], either **3-D PhypI** (Figures 5 and S1–S4) or **3-D PhypII** (Supplementary Materials Figures S5–S9) features were superimposed with the derived steric and electrostatic **PLS-coefficients** and jointly interpreted. The models' robustness was monitored through leave-one-out (LOO) and leave-some-out (LSO) cross-validations (CV) (Figure 4 and Supplementary Material Tables S3–S6) [80,92], whereas any lack of chance correlation was confirmed by employing Y-scrambling (Y-S) [80,92].

Table 4. The alignment of best hypotheses pharmacophoric features (**A**: hydrogen-bond acceptor, **D**: hydrogen bond donor, **R**: ring feature, **H**: hydrophobic feature, **P**: positive ionizable feature) against **1ERR** (blue) and **1ERE** (pink). Scores of the different parameters (the upper part) and PLS statistical parameters (the lower part) of the top two hypotheses.

ADDRRRP.11						ADDHHHP.13					
											
HID ^a	S ^b	S-I ^c	P-H ^d	S ^e	V ^f	VOL ^g	SE ^h	M ⁱ	A ^j	I ^k	
ADDRRRP.11	3.741	0.967	6.429	0.81	0.991	0.426	2.678	17	9.52	1.751	
ADDHHHP.13	3.743	0.963	6.432	0.83	0.993	0.431	2.674	17	9.30	1.755	
	PLSF ^l	r ^{2m}	SD ⁿ	F ^o	P ^p	Stability ^q	q ² LOO ^r	q ² LSO ^s	q ² YS LOO ^t	q ² YS LSO ^u	
ADDRRRP.11	5	0.949	0.264	61.3	4.38e ⁻¹⁵	0.971	0.825	0.627	-0.234	-0.247	
ADDHHHP.13	5	0.951	0.257	61.4	4.41e ⁻¹⁵	0.977	0.826	0.659	-0.241	-0.258	

^a Hypothesis identification; ^b Survival score; ^c Survival-inactives score; ^d Post-hoc—the result of rescaling; ^e Site score—an RMDS value for the site points superimposition in an alignment to the pharmacophore of the structures that contribute to this hypothesis; ^f Vector alignment score; ^g Volume of the contributing structures' overlap when aligned on the pharmacophore; ^h Selectivity—the fraction of molecules matching the hypothesis regardless of their potency; ⁱ Matches—number of actives that match the hypothesis; ^j Activity—Activity of the reference ligand (pIC₅₀); ^k Inactive—Survival score of inactives; ^l PLS factor, i.e., $N/5$, where N is the number of ligands present in the training set; ^m Conventional square-correlation coefficient. ⁿ Standard deviation of regression; ^o Ratio of the model variance to the observed activity variance; ^p Significance level of variance ratio; ^q Stability of the model predictions to changes in the training set composition; ^r Cross-validation correlation coefficient using the leave-one-out (LOO) method. ^s Cross-validation correlation coefficient using the leave-some-out (LSO) method with 5 random groups; ^t Average cross-validation correlation coefficient using the leave-one-out (LOO) method obtained after Y-scrambling process. ^u Average cross-validation correlation coefficient using the leave-some-out (LSO) method with 5 random groups obtained after the Y-scrambling process.

The **D₁/RED_{PLS-coefficients}** (Figures 5 and S1–S9) emphasized that the ER α binder should possess the mixed hydrogen bond donating (HBD)/hydrogen bond accepting (HBA) functional group (like the frequently present aromatic hydroxyl group, i.e., **1st PhOH**, as in **1ERR**, Table 1, Figure 5A, [13]), to form hydrogen bonds (HBs) with H3 Glu353 and H6 Arg394, at the same time not too voluminous, according to the **YELLOW_{PLS-coefficients}** maps.

The **D₂** feature/**GREEN_{PLS-coefficients}**/**RED_{PLS-coefficients}** (Figures 5 and S1–S4) indicated that another, *p*-positioned HBD/HBA functional group (i.e., **2nd PhOH**, as found in **1ERR**, Table 1, Figure 5A, [13]) is required to form HB with H11 His524 [17–20].

The **H₁ (R₁)** feature/**GREEN_{PLS-coefficients}**/**YELLOW_{PLS-coefficients}** (Figures 5 and S1–S9) suggested that the **1st PhOH** and **2nd PhOH** should be interconnected with five-membered (**1ERP1**, Table 1, Figures 6A and S5A [13]) or six-membered heterocyclic aliphatic bridge (**1XP1**, Table 1, Figures 6C and S5C [64]), to interact with H6 Met388 H6-to-H7 loop residues Phe404, Ile424, and Leu428, maintaining the voluminosity toward distinct residues as low as possible [66]; according to the **BLUE_{PLS-coefficients}**, the bridge may be improved by means of an HBD, to face H3 Glu353 or H3 Thr347 (see **1XP1**, Table 1, Figure 5C [64]).

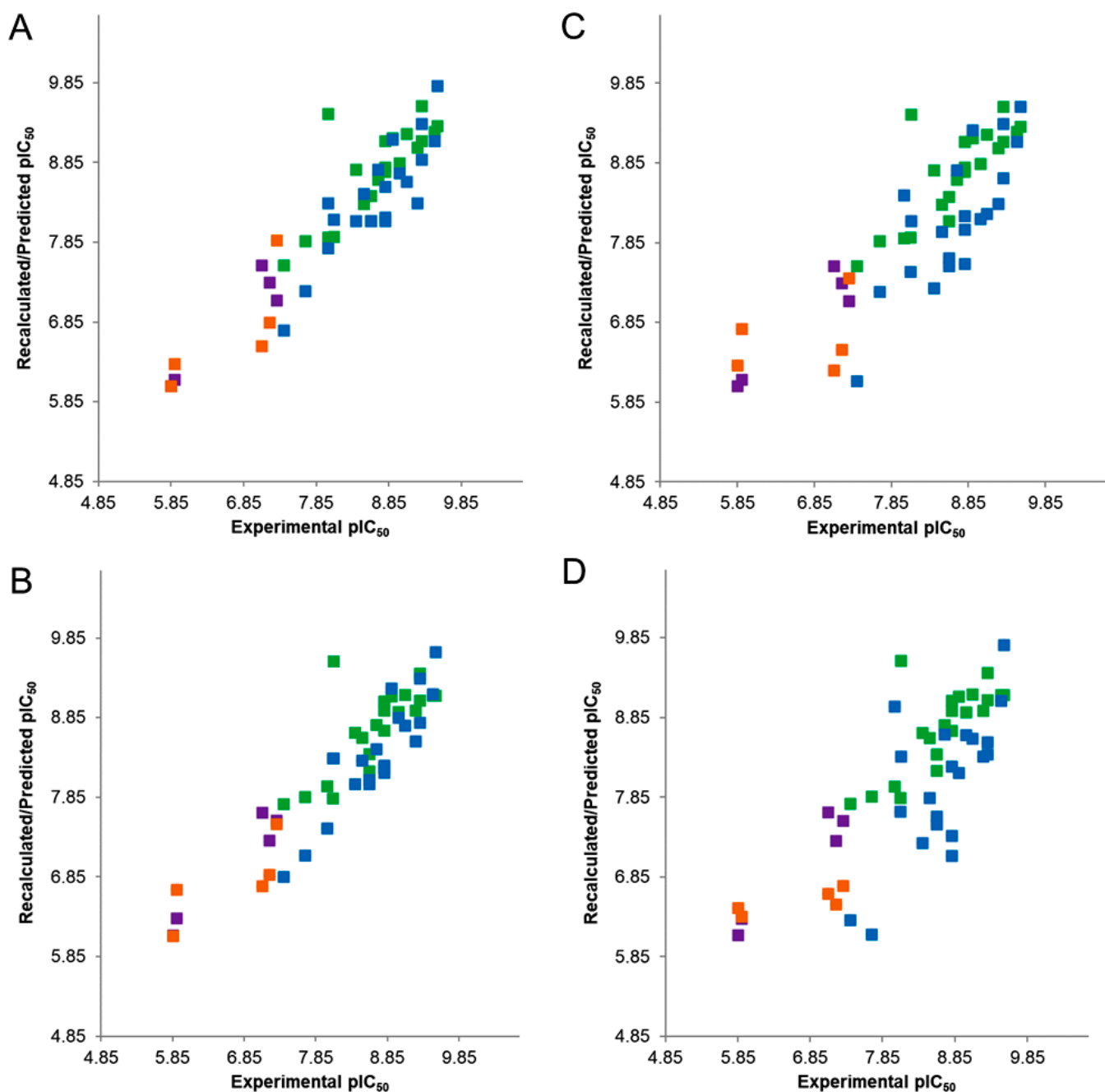


Figure 4. Experimental vs. recalculated (“actives”: green squares; “inactives”: purple squares) and predicted (“actives”: blue squares; “inactives”: orange squares) pIC₅₀s for **ADDHHHP.13** hypothesis and LOO cross-validation (A); **ADDRRRP.11** hypothesis and LOO cross-validation (B); **ADDHHHP.13** hypothesis and LSO cross-validation (C); **ADDRRRP.11** hypothesis and LSO cross-validation (D).

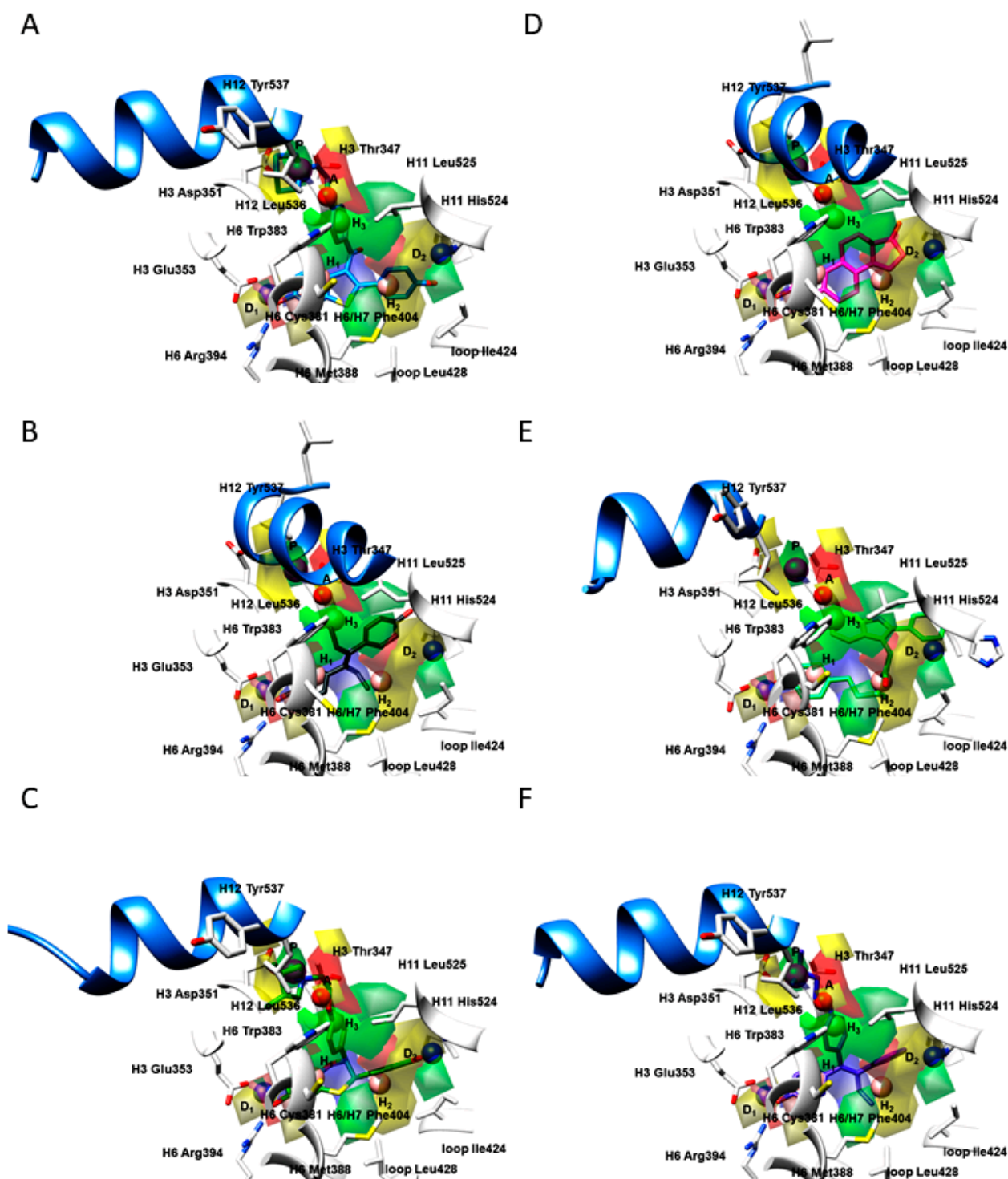


Figure 5. The 3-D PhypI features (D: hydrogen-bond donors, A: hydrogen-bond acceptors, H: hydrophobic features, P: positive ionizable features) and 3-D QSAR *PLS-coefficients* contour maps (*GREEN_{PLS-coefficients}*: positive steric interactions, *YELLOW_{PLS-coefficients}*: negative steric interactions, *BLUE_{PLS-coefficients}*: areas where positively charged functional groups and H-bond donors are favored whereas the negatively charged functional groups and H-bond acceptors are disfavored, *RED_{PLS-coefficients}*: areas negatively charged functional groups and H-bond acceptors are favored, whereas the positively charged functional groups and H-bond donors are disfavored) for **1ERR** (A); **3ERD** (B); **1XP1** (C); **1ERE** (D); **2IOK** (E); **2BJ4** (F). Amino acid residues are depicted in white. For the clarity of presentation, only the H12 helix is presented in a cornflower blue ribbon, as a crucial delimiter for partial agonists, SERMs, and SERDs.

The **H₂ (R₂)** feature/**GREEN**_{PLS-coefficients}/**YELLOW**_{PLS-coefficients} (Figures 5 and S1–S9) indicated that the chemical linker between the **1st PhOH** and the **2nd PhOH** should not be further degraded (for instance toward the ethyl group of **3ERD** [69], Table 1, Figures 5B and S5A), to avoid ER α partial agonism and pure ER β antagonism and that the bulkiness of **2nd Ph-OH** toward H6 Met388 and H6-to-H7 loop residues Phe404, Ile424, and Leu428 is sufficient as is.

The **H₃ (R₃)** feature/**GREEN**_{PLS-coefficients}/**RED**_{PLS-coefficients} (Figures 5 and S1–S9) indicated that SERMs and SERDs, differently from partial agonists and ER β selective binders (**3ERD** [69], Table 1, Figures 5B and S5A), should possess a central phenyl ring, hereinafter labeled as **Ph** (see **1ERR**, Table 1, Figure 5A) [13] and **1XP1**, Table 1, Figure 5C [64]) to sterically interact with the H3 Thr347 side chain methyl group and alleviate the H3 Thr347-H11 Leu525-H12 Leu536 hydrophobic network formation (stabilized by the auxiliary H3 Ala350-**Ph**-H11 Leu525 network) [13]. The bulkiness of **Ph** could be increased toward H6 Trp383 (note the **GREEN**_{PLS-coefficients}), whereas the *o*-hydrophobic/HBA substituents of **Ph** could activate Thr347's side-chain hydroxyl group (see **GREEN**_{PLS-coefficients}/**RED**_{PLS-coefficients}).

The **A** feature and **RED**_{PLS-coefficients}/**YELLOW**_{PLS-coefficients} (Figures 5 and S1–S9) emphasized the electrostatic interactions of an ethanolamine's oxygen atom (hereinafter labeled as **Oxy**), an extension of **Ph** (Tables 1 and 2) with the H3 Thr347's side-chain -OH group.

The **P** feature/**BLUE**_{PLS-coefficients}/**GREEN**_{PLS-coefficients}/**YELLOW**_{PLS-coefficients} (Figures 5 and S1–S9, see Supplementary Materials) discriminated SERMs from SERDs. Hence, SERMs (Tables 1 and 2) should form an HB with H3 Asp351 by means of an HBD, such as the positively charged nitrogen within heterocyclic and aliphatic scaffolds of low(er) voluminosity (see **1ERR**, **1SJ0**, **1YIN**, **2R6W**, and **1UOM**, Figures 5A, S1B,F and S2B, respectively) [2,13,61,73], **1XP1** (Figure 5C) [64], **1XP6** (Supplementary Materials Figure S1A) [64], **2R6Y**, **1XP9**, **1YIM**, and **1XPC** (Supplementary Materials Figures S1C–E and S2A) [26,28,36], **2IOK** and **2IOG** (Figures 5E and 6C) [68], and **1XQC** (Supplementary Materials Figure S3B) [65]), to stabilize the H12 in the open conformation [6,10,13,64], at the same time keeping the steric pressure toward H12 at minimum or reducing it. On the other hand, SERDs (Tables 1 and 2) should form an HB with H3 Asp351 via the HBA/HDB portion (like carboxylic acid within the phenyl acrylic acid (as in **1R5K**, Supplementary Materials Figure S2D [59] and **5AK2**, Figure 6B [74]), to provoke the proteasomal degradation of ER α [17–20].

2.3. Predictive Ability Assessment of the 3-D PhypI/3-D QSAR Model Ensemble

To validate the **3-D PhypI/3-D QSAR model**'s predictive ability, the TS_{CRY} (Tables 3 and 5) (Refs. [69,75–79]) and TS_{MOD1}-TS_{MOD3} (Supplementary Materials Tables S10–S15) [94–102] were used. For the sake of the reader, only the predictions of TS_{CRY} are herein discussed. Using a consensus score strategy [80,91,92], the bioactive conformations of modeled compounds [103] within the TS_{MOD1}-TS_{MOD3} (see the section Predictive ability assessment of the 3-D PhypI/3-D QSAR model ensemble), were obtained using SB [104–107] or LB alignment [80,91,92], as described in the Supplementary Material (see Supplementary Materials Alignment assessment rules, Structure-based alignment assessments, and Ligand-based alignment assessments sections, as well as Tables S7–S9 and Figures S10–S19).

TS_{CRY}'s experimentally available binding conformation's pK_i values (herein improperly assumed as pIC₅₀s) were thereafter predicted with an average absolute error of predictions (AAEPs) of 0.66 and 2.35 for the model optimized with LOO and LSO CVs, respectively (Table 5) and associated predictive q^2 (q^2_{pred}) values were 0.51 and 0.39, respectively. Interestingly and as expected, the SB re-aligned molecules were predicted with lower errors (q^2_{pred} /AAEP values of 0.46/1.27 and 0.46/1.27 for LOO and LSO derived models) than those LB re-aligned (q^2_{pred} /AAEP values of 0.29/1.37 and 0.31/1.40 for LOO and LSO derived models). These values indicated the good predictive ability [108–110] of the **3-D PhypI/3-D QSAR model** ensemble and support the goodness of the realignment methodology.

Table 5. Summary of the 3-D PhypI/3-D QSAR model ensemble experimental/structure-based/ligand-based predictive ability for TS_{CRY}.

Entry	pK _i	EC Pred. pK _i ^a		AAEP ^d	SB Pred. pK _i ^a		AAEP ^d	LB Pred. pK _i ^a		AAEP ^d
		LOO ^b	LSO ^c		LOO ^b	LSO ^c		LOO ^b	LSO ^c	
3ERT	9.60	8.76	8.64	0.90	8.36	8.34	1.25	7.99	8.12	1.55
3UU7	8.79	8.14	6.91	1.27	8.09	7.22	1.14	7.85	7.14	1.30
3UUA	8.79	8.15	7.54	0.94	7.05	7.12	1.71	8.07	7.37	1.07
3UUC	5.70	4.36	4.39	1.33	4.45	4.06	1.45	5.67	6.77	0.55
4DMA	5.60	6.54	7.69	1.52	7.91	7.59	2.15	8.86	7.7	2.68
4MG6	6.00	4.76	4.77	1.24	4.17	3.03	2.40	4.16	4.82	1.51
4MG8	10.00	8.86	8.87	1.14	9.16	7.76	1.54	8.99	8.85	1.08
4MG9	6.00	7.12	6.52	0.82	6.19	4.10	1.05	4.51	5.96	0.77
4MGA	6.00	8.13	6.99	1.56	7.13	6.89	1.01	7.41	4.98	1.22
4MGC	7.00	8.66	6.7	0.98	6.36	6.54	0.55	7.58	5.85	0.87
4MGD	6.00	7.66	9.04	2.35	8.46	7.13	1.80	9.19	9.48	3.34
4TUZ	10.00	8.64	8.88	1.24	9.17	7.52	1.66	9.06	8.7	1.12
4ZN9	9.60	8.96	8.92	0.66	8.74	7.06	1.70	8.78	8.49	0.97

^a Predictions were obtained with a 3-D PhypI/3-D QSAR model ensemble optimized with LOO and LSO cross-validations. ^b Leave-one-out cross-validation. ^c Leave-some-out cross-validation with 5-random-groups-out. ^d AAEP, the average absolute error of prediction of LOO and LSO cross-validations.

2.4. Virtual Screening, Anticancer Potency, and Binding Mode Analysis of Brefeldin A as a Hit for Hit-to-Lead Optimization towards Innovative SERMs

The 3-D PhypI/3-D QSAR model coupled with SB/LB alignment rules was used to perform a virtual screening (SB/LB VS) [87,90] on 4411 compounds taken from the National Cancer Institute (NCI). The top-ranked 18 virtual hits (See Supplementary Materials: Virtual screening, Table S16, and Supplementary Materials Figures S20–S22), with either SB or LB predicted pIC₅₀ values, were experimentally validated as either ER α binders or antiproliferative agents against MCF-7, MDA-MB-231, and MRC-5 cell lines (Supplementary Materials Table S17). Compound coded as NCI89671, a naturally occurring compound Brefeldin A (BFA, Figure 6A) [111], as the most potency predicted, did exert promising activity against ER α (IC₅₀ of 8.34 μ M) and the MCF-7 cell line (IC₅₀ of 9.01 μ M), and selectivity against the MDA-MB-231 cell line (selectivity index (SI) of 11.10), although less potent than the references E₂ [13], 4-hydroxytamoxifen (4-OHT) [32], and raloxifene (Ral) [13] (Supplementary Materials Table S17). Previously assessed anti-BC properties of BFA and its derivatives were associated with the apoptosis and the compounds' ability to disrupt the *cis*-Golgi apparatus [112,113]. Interestingly, C4- and C7-esters of BFA exerted nM antiproliferative activity against MCF-7 cell lines [114], C4-succinyl, glutaryl BFA analogs, and C7-long lipids derivatives showed μ M to nM potencies against MCF-7 cell lines [115], whereas the sulfide- and sulfoxide-conjugated BFA analogs were active against MDA-MC-435 cell lines as μ M and sub-micromolar ranges [116].

BFA binding mode analysis showed an interaction profile as a putative partial agonist, likely inducing the H12 in a closed conformation (Figure 6B) [13]. Thus, the BFA's cyclopentane ring and the C7-OH group formed H-bonds with H3 Glu353 and H6 Arg394 (d_{HB} = 2.855 and 2.990 Å, respectively). Moreover, the C4-OH portion established the electrostatic interactions with H3 Glu353. On the other hand, the close contact of the C15-CH₃ with H11 His524 was accounted as unfavorable by the 3-D PhypI/3-D QSAR model ensemble, suggesting the insertion of either HBA or HBD functionality. Consequently, the C1-to-C4 carbon atoms were interfaced to H12, whereas the C9-to-C15 skeleton was engaged in van der Waals interactions with H6 Met388 and H6-to-H7 loop residues Ile423 and Leu428. Finally, the C1 carbonyl group was observed away from any interesting interactions, not satisfying any 3-D PhypI/3-D QSAR model features, indicating it as a possible substitution point into an HBA group. Hence, the 3-D PhypI/3-D QSAR model ensemble indicated that the modification of the C15-CH₃ into C15-OH could endow BFA's horizontal flip toward Glu353/Arg394, at the same time positioning the cyclopentane ring's C7-OH

group toward the His524 (an alignment comparable to the E₂'s D ring and C17-OH group experimental conformation [13]). In such a scenario the C1 carbonyl group would face Glu353 and the C-4 OH group would become a further anchor point for the implementation of a Ph-containing scaffold.

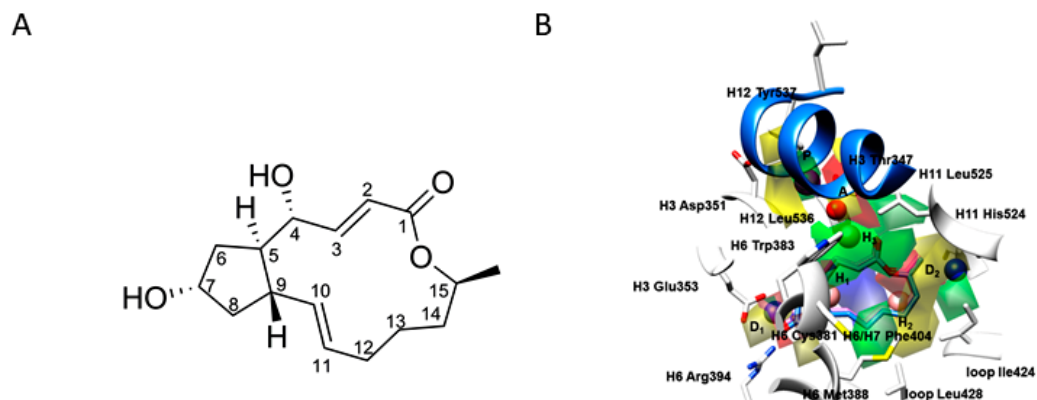


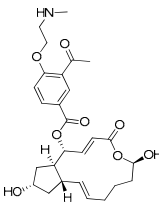
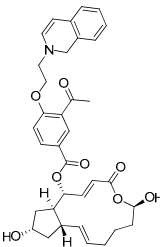
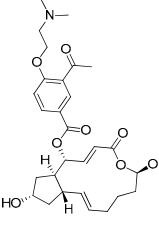
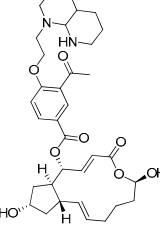
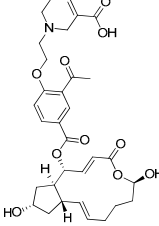
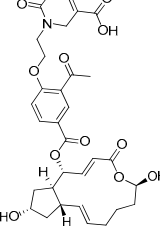
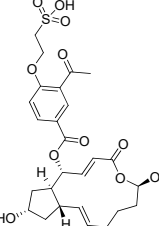
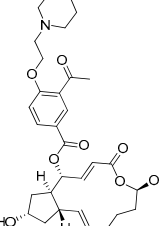
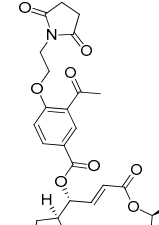
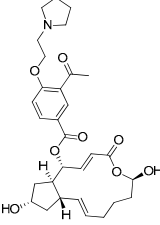
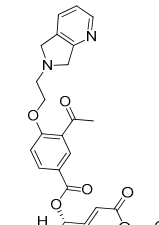
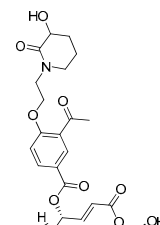
Figure 6. The NCI89671 (viz., BFA) structure and nomenclature (A); the SB/LB virtually screened conformations of NCI89671, SB conformation blue, LB conformation pink (B).

2.5. Rules for the Rational Design of Novel Brefeldin A Derivatives as SERMs

The BFA structural optimization toward novel ER α SERMs (Table 6) was thereafter performed by applying the guidelines from the 3-D PhypI/3-D QSAR model ensemble, applicable only for the rational design of SERMs. The *partial agonist-to-SERM* conversion was undertaken by applying the following strategies:

1. The BFA's C15-CH₃ group was converted to C15-OH as a mixed HBA/HBD functional group to increase the compounds' capacity for establishing hydrogen bonds with either H3 Glu353 and H6 Arg394 (or H11 His524) and hopefully the solubility (data not shown).
2. The BFA's C4-OH was substituted with 3-acetyl-4-hydroxybenzoic acid to provide interactions with H6 Trp383 and H3 Thr347, as well as to stabilize the H3 Thr347-Leu525-H12 Leu536 hydrophobic network, and consequent H12 dislocation. Choosing 3-acetyl-4-hydroxybenzoic acid as a BFA's C4-OH substituent was an experimentally-guided decision since the tentative attempts to synthetically incorporate (see further text) the 1-(1,4-dihydroxynaphthalen-2-yl)ethenone as a fragment, perhaps more suitable to target H6 Trp383 by means of steric interactions, failed.
3. The 3-acetyl-4-hydroxybenzoic acid's *p*-OH was further substituted with either ethanolamine-based moieties, bearing primary and secondary amines, or various *N*-, *O*-, and *N*, *O*-heterocycles or 2-hydroxyethanesulfonic acid functions, capable of inducing the AF-2 function dislocation. The primary amine, secondary amine, and 2-hydroxyethanesulfonic acid were chosen as the AF-2 function invaders to reduce the steric pressure on H12, at the same time with the eligibility to establish HBs with H3 Asp351. On the other hand, as the 3-D PhypI/3-D QSAR model ensemble was not explicit on whether to keep the steric pressure on H12 or to reduce it completely, the various *N*-, *O*-, and *N*, *O*-heterocycles were chosen as bioisosteres of heterocycles found within the ER α binders (Tables 1 and 2) in a way that their HBD functional groups could primarily engage H3 Asp351, thus influencing, alongside the steric pressure, the H12's induced fitting, whereas the existing HBA functional groups could produce additional favorable interactions with the surrounding residues.

Table 6. Structures of designed hits and their predicted activities against ER α .

#	Ligand Structure	3DPhypI/3-D QSAR pred. pIC ₅₀ SB ^a	LB ^b	#	Ligand Structure	3DPhypI/3-D QSAR pred. pIC ₅₀ SB ^a	LB ^b
3DPQ-1		9.20	9.17	3DPQ-7		9.26	9.11
3DPQ-2		9.21	9.12	3DPQ-8		9.04	8.95
3DPQ-3		9.37	9.29	3DPQ-9		9.31	9.26
3DPQ-4		9.26	9.22	3DPQ-10		9.18	9.05
3DPQ-5		9.05	8.92	3DPQ-11		9.12	9.28
3DPQ-6		9.01	8.91	3DPQ-12		9.42	9.35

^a The designed compounds SB predicted activities by the 3DPhypI/3-D QSAR model; ^b The designed compounds LB predicted activities by the 3DPhypI/3-D QSAR model.

- The 12 designed compounds, belonging to the **3-D PhypI/3-D QSAR**-based series, viz., **3DPQ**, were then subjected to the SB/LB alignment (Supplementary Materials Figures S23 and S24) and the pIC₅₀ prediction procedures against ER α (Table 6). This way, the designed compounds composed the ultimate prediction set [109,110] for the **3-D PhypI/3-D QSAR model** ensemble, in which the SB and LB models' associated q^2_{pred} and AAEP values were 0.858/0.045 and 0.732/0.1, respectively. Indeed, even eight compounds, namely **3DPQ-12**, **3DPQ-3**, **3DPQ-9**, **3DPQ-4**, **3DPQ-2**, **3DPQ-1**, **3DPQ-7**, and **3DPQ-11** were predicted as more potent than **1ERR** [13] (the most potent TR compound; see further text).

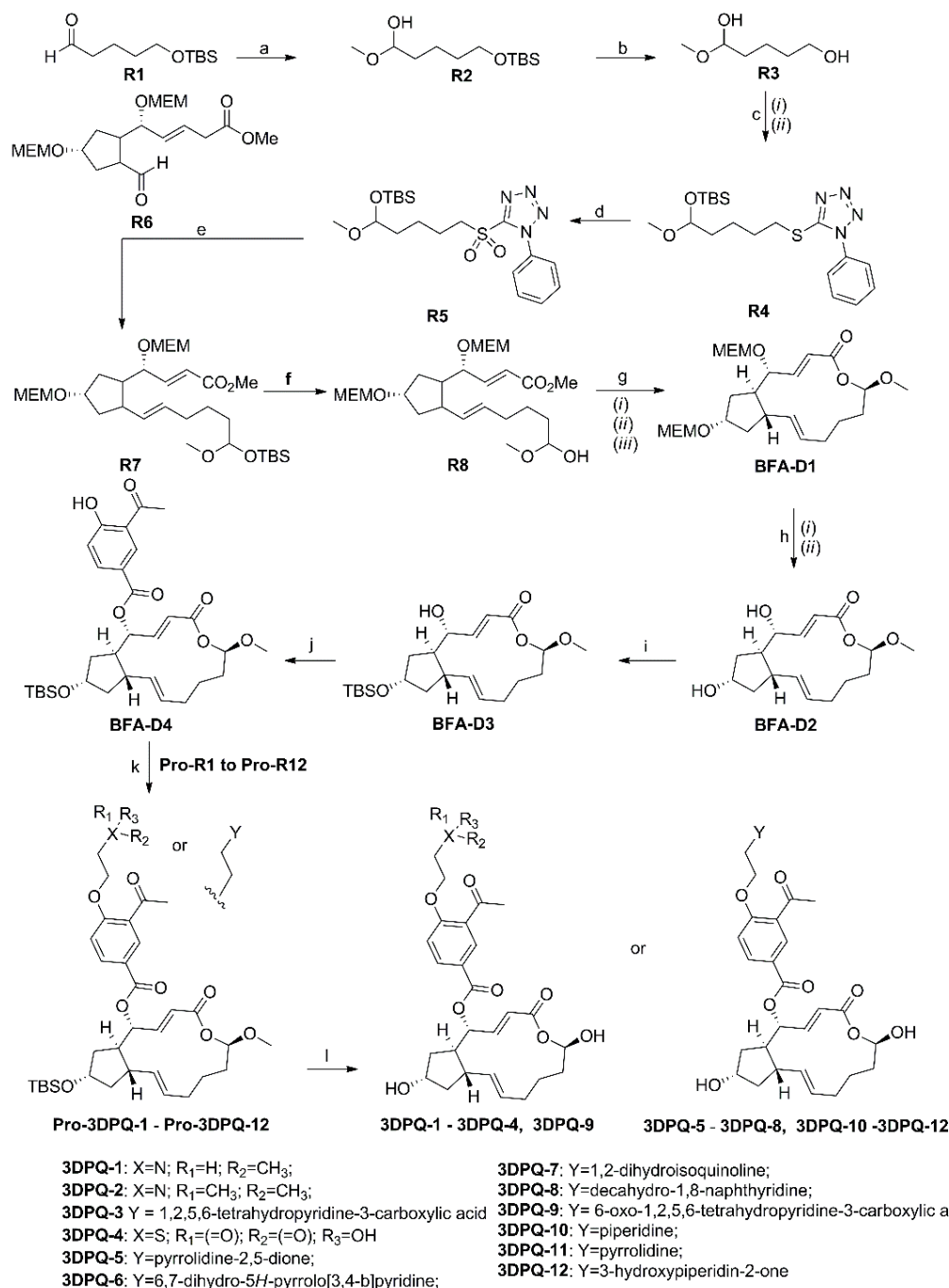
2.6. Synthesis of Brefeldin A Derivatives 3DPQ-1 to 3DPQ-12

Designed compounds **3DPQ-1** to **3DPQ-12** were synthesized in high yields and purities (Scheme 1). The synthetic protocols and associated ¹H NMR, ¹³C NMR, ¹⁵N NMR, and ¹⁷O NMR spectral data, as well as the HPLC spectra confirming compounds' purity of 95% and higher, are reported in Supplementary Materials (Synthetic protocols for the preparation of compounds **3DPQ-1** to **3DPQ-12**, Synthesized Compounds spectral data interpretation, Supplementary Materials Figures S26–S190).

Thus, the building of a **BFA**-like core started with the previously reported two-step conversion of 1,5-pentanediol towards the aldehyde **R1** (87% yield), containing the aldehyde functional group at position C1-OH and *tert*-butyldimethylsilyl chloride (TBS-Cl)-protected C5-OH portion [117]. Following this, **R1** was converted into **R2** (88% yield), an intermediate containing the single-methylated hydroxyl group within the geminal diol sub-structure as a forebear of what would be the **BFA**'s C15 methyl group: the conversion occurred upon the asymmetric addition of dimethylzinc using the (-)-1,8-diazabicyclo [5.4.0]undec-7-ene ((-)-DBNE) as chiral ligand at a reaction temperature of 0 °C; the **R2** was purified by silica gel flash chromatography (Et₂O:EtOAc = 10:1 *v/v* as eluent) [118]. Afterward, **R2** was TBS-deprotected with 1N HCl to give **R3** (95% of yield), further converted to the 1-phenyl-1*H*-tetrazole-5-thiol derivative **R4** (70% of yield) using a Mitsunobu reaction that assumed: (i) the protection of the free hydroxyl group of the geminal diol sub-structure by TBS-Cl; (ii) the addition of 1-phenyl-1*H*-tetrazole-5-thiol in dry THF to the deprotected C5-OH of **R3**, as well as the inclusion of TBS-Cl in imidazole and 4-(dimethylamino)pyridine (DMAP) onto the free hydroxyl group of the geminal diol (the product was purified using silica gel flash chromatography (Et₂O:EtOAc = 40:1 *v/v* as eluent)) [114]. Following this, the Mo(VI)-catalyzed oxidation of **R4** produced tetrazolyl sulfone **R5** (75% of yield), refined by silica gel flash chromatography (Et₂O:EtOAc = 2:1 *v/v* as eluent) [119] and further subjected to Julia–Kocienski olefination with **R6** (prepared as described elsewhere in 67% yield [119,120] and containing the MEM-protected hydroxyl groups), using potassium hexamethyldisilazane (KHMDs) in toluene as a base, to give *E*-olefin **R7** in 73% yield [121,122]. Subsequently, the selective deprotection of TBS-OH within the geminal diol with 1N HCl gave **R8** (89% yield), purified by silica gel flash chromatography (Et₂O:EtOAc = 3:1 *v/v* as eluent) [114].

R8 was then subjected to the Yamaguchi lactonization, furnishing **BFA-D1** (88% yield) [123]. In particular: (i) the **R8**'s methyl ester (the functionality originating from **R6**) was hydrolyzed with 1N LiOH; (ii) the Yamaguchi reagent (2,4,6-trichlorobenzoyl chloride) was added to the carboxylic acid, in the environment of NEt₃, resulting in the formation of an intermediate anhydride (not isolated); (iii) the reaction of the anhydride with the hydroxyl group of the geminal diol in the presence of DMAP generated the lactone **BFA-D1**, where the **BFA**'s C15 methyl group was successfully transformed into the methoxy one. Subsequently, the MEM-protecting groups were removed from **BFA-D1** with HBr [124], and the obtained **BFA-D2** was purified by silica gel flash chromatography (Et₂O:EtOAc = 1:1 *v/v* as eluent) and recrystallized from MeOH in 75% yield [114]. Subsequently, the **BFA-D2**'s C7-OH group was protected with *tert*-butyldimethylsilyl trifluoromethanesulfonate (TBSOTf) in 2,6-lutidine to form **BFA-D3** in moderate yield (25%, purified by silica gel flash chromatography (*n*-hexane:EtOAc = 8:2 *v/v* as eluent) [114]. The **BFA-D3**'s C4-OH

was afterward subjected to esterification with 3-acetyl-4-hydroxybenzoic acid, in the presence of 1-ethyl-3-(3-dimethylaminopropyl) carbodiimide hydrochloride (EDAC·HCl) and DMAP, and in the prolonged reaction time (24 h), to give **BFA-D4**, purified by column chromatography on silica gel (*n*-hexane:EtOAc = 1:1 *v/v* as eluent) [125].



Scheme 1. Synthesis of Brefeldin A derivatives **3DPQ-1** to **3DPQ-12**. Reagents and conditions: (a) Me₂Zn, (–)-DBNE, toluene, 0 °C, 24 h, 87% ee; (b) HCl, THF, rt, 25 min; (c) (i) TBS-Cl, imidazole, DMAP, CH₂Cl₂, 0 °C, 3 h, (ii) PPh₃, DEAD, 1-phenyl-1*H*-tetrazole-5-thiol, THF, 0 °C, 16h; (d) (NH₄)₆Mo₇O₂₄, H₂O₂, EtOH, rt, 16 h; (e) compound R6, KHDMS, 1,2-dimethoxyethane; -78 °C, 18h; (f) HCl, THF, rt, 1.5 h; (g) (i) LiOH, THF/H₂O, rt, 2h, (ii) 2,4,6-trichlorobenzoylchloride, NEt₃, THF, rt, 1.5 h, (iii) DMAP, toluene, reflux, 5h; (h) (i) cc HBR, THF, rt, 1.5 h (ii) recrystallization; (i) TBSOTf, 2,6-lutidine, CH₂Cl₂, rt; (j) 3-acetyl-4-hydroxybenzoic acid, ECD, DMAP, CH₂Cl₂, reflux; (k) K₂CO₃, EtOH, reflux; (l) (i) TBAF, THF, rt, (ii) BBr₃, CH₂Cl₂, 0 °C, 3h, reflux.

The **BFA-D4'**'s *p*-OH moiety then was equimolar alkylated with either commercially available pro-reagents **Pro-R1**, **Pro-R2**, **Pro-R4**, **Pro-R5**, **Pro-R10**, and **Pro-R11** (i.e., 2-chloro-*N*-methylethanamine, 2-chloro-*N,N*-dimethylethanamine, 2-chloroethanesulfonic acid, 1-(2-chloroethyl)pyrrolidine-2,5-dione, 1-(2-chloroethyl)piperidine, and 1-(2-chloroethyl)pyrrolidine, respectively), or with prepared **Pro-R3**, **Pro-R6**, **Pro-R7**, **Pro-R8**, **Pro-R9**, and **Pro-R12** (i.e., 1-(2-chloroethyl)-1,2,5,6-tetrahydropyridine-3-carboxylic acid, 6-(2-chloroethyl)-6,7-dihydro-5*H*-pyrrolo [3,4-*b*]pyridine, 2-(2-chloroethyl)-1,2-dihydroisoquinoline, 1-(2-chloroethyl)decahydro-1,8-naphthyridine, 1-(2-chloroethyl)-6-methylene-1,2,5,6-tetrahydropyridine-3-carboxylic acid, and 1-(2-chloroethyl)-3-hydroxypiperidin-2-one, respectively), in the environment of potassium carbonate under reflux, to give **Pro-3DPQ-1** to **Pro-3DPQ-12** [126]. Subsequent deprotection of compounds' C7-OH, with *tert*-butylammonium fluoride in THF [114], and C15-OH groups, using the complete demethylation of C15-OH using the boron tribromide (2 equiv. per methoxy function) in dry dichloromethane at 0 °C [127], finally gave the designed compounds **3DPQ-1** to **3DPQ-12**.

2.7. Synthesized Compounds Antagonistic Potency and Relative Binding Affinities against ER α and ER β

The **3DPQ-1** to **3DPQ-12** were then investigated for their potency to antagonize either ER α (Table 7 and Supplementary Materials Figures S191 and S192) or ER β (Table 7 and Supplementary Materials Figures S193 and S194) [128,129]. The experimentally determined IC₅₀ values for **3DPQ-1** to **3DPQ-12** against ER α (Table 7) were highly correlated to those predicted by the 3-D PhypI/3-D QSAR model ensemble (Table 6). Compounds **3DPQ-12**, **3DPQ-3**, **3DPQ-9**, **3DPQ-4**, **3DPQ-2**, **3DPQ-1**, **3DPQ-7**, and **3DPQ-11** were more potent ER α antagonists than both **Ral** and **4-OHT**, exerting potency in the pM range. All the compounds were potent ER α binders and poor ER β binders (see logRBA values Table 7).

Compared to **BFA**, in all the synthesized compounds, the C15-CH₃ to C15-OH conversion seemed to participate in an ER α 's LDB main core horizontal flipping (Figures 7 and S195). Thus, the C15-OH faced the H3 Glu353 and H6 Arg394 to establish two further HBs (see Supplementary Materials Table S18 for details). Consequently, the C1 carbonyl portion produced weak electrostatic interactions with H6 Trp383's indole ring nitrogen. The C8-C15 carbon skeleton was observed to be sterically attracted by H6 Met388 and H6-to-H7 loop residues Ile423 and Leu428. The inverse alignment of the main core influenced the spatial positioning of the cyclopentane ring's C7-OH, as well, which produced HBs with H11 His524 (see Supplementary Materials Table S18 for details). The remaining C1-C4 carbon backbone participated in steric hindrance with H6 Trp383. Furthermore, the esterification of the C4-OH portion with 3-acetyl-4-hydroxybenzoic acid influenced the H3 Thr347-H11 Leu525-H12 Leu536 hydrophobic network [13,69] formation: the ester oxygen electrostatically targeted the H11 His524 side chain, while the *p*-carbonyl group made H-bonds with H3 Thr347's side-chain hydroxyl (see Supplementary Materials Table S18 for details); the incorporated *o*-Ac-Ph moiety formed eclipsed (i.e., edge to edge) van der Waals interactions with the H3 Thr347's side chain methyl group using its own methyl group, as well as the additional HBs with H3 Thr347's side chain hydroxyl group (see Supplementary Materials Table S18 for details) by the acetyl group carbonyl portion. The unsubstituted 3-acetyl-4-hydroxybenzoic ac carbons faced the H12 Leu536 in a T-shaped fashion. Furthermore, the *p*-O-CH₂-CH₂- bridge bore the **3DPQ-1**'s to **3DPQ-12**'s functionalities that forced the H12 drifting, at the same time establishing the electrostatic attraction with H3 Thr347's hydroxyl group via the oxygen atom and the steric interactions between the methylene carbons and the Leu536 isobutyl group.

The activity and SERM pharmacology [13] of **3DPQ-12** (Table 7, Supplementary Materials Figure S191A, Figure 7A, potency 1.85-fold higher than **Ral**) could be also ascribed to the 3-hydroxypiperidin-2-one portion: positioned beneath the Asp351-Leu536 plane, its hydroxyl group established an HB with Asp351 (the $d_{\text{HB}} = 3.112 \text{ \AA}$), stabilizing ER α with H12 in the open conformation; the carbonyl group electrostatically interfered with the Thr347's side chain hydroxyl group, whereas the carbon skeleton was in the proximity

of Leu536 isobutyl group. A slightly less potent SERM, for just 0.04 nM, was the **3DPQ-3** (Table 7, Supplementary Materials Figure S191B, Figure 7B, potency 1.68-fold higher than **Ral**), whose 1,2,5,6-tetrahydropyridine-3-carboxylic acid scaffold formed an HB with Asp351 (the $d_{\text{HB}} = 3.222 \text{ \AA}$) via the carboxyl group, whereas the carbon skeleton behaved similarly as in **3DPQ-12**. Furthermore, the potency of **3DPQ-9** (Table 7, Supplementary Materials Figure S191C, Figure 7C, 1.64-fold stronger binder than **Ral**), decreased by 0.01 nM related to **3DPQ-3** with the introduction of the carbonyl portion at position C6 of 1,2,5,6-tetrahydropyridine-3-carboxylic acid, which electrostatically attracted the Trp383's indole ring nitrogen, having a consequence in C3-COOH group dispositioning and a weaker HB with H3 Asp351 (the $d_{\text{HB}} = 3.314 \text{ \AA}$).

Table 7. Antagonistic potencies (IC_{50} s) and the logarithm of the relative binding affinities (RBA) against $\text{ER}\alpha$ and $\text{ER}\beta$ of the newly synthesized compounds. Isoform affinity preferences and respective antagonist constants are also reported.

Comp.	$\text{ER}\alpha^a$ (IC_{50} nM)	$\text{ER}\beta^b$ (IC_{50} nM)	$\log\text{RBA}^c$ $\text{ER}\alpha$	$\log\text{RBA}^d$ $\text{ER}\beta$	$K_a \text{ER}\alpha^e$ (nM)	$K_a \text{ER}\beta^f$ (nM)
3DPQ-1	0.57 ± 0.54 §, †, ‡, §	74.33 ± 0.46 †, ‡, §	2.19 †, §	0.08 †, ‡, §	0.13 †, ‡	41.76 †, ‡, §
3DPQ-2	0.54 ± 0.31 †, ‡, §	77.24 ± 0.42 †, ‡, §	2.22 †, ‡, §	0.06 †, ‡, §	0.12 †, ‡	43.39 †, ‡, §
3DPQ-3	0.44 ± 0.31 †, ‡, §	74.86 ± 0.14 †, ‡, §	2.31 †, ‡, §	0.08 †, ‡, §	0.10 †, ‡	42.06 †, ‡, §
3DPQ-4	0.47 ± 0.12 †, ‡, §	82.45 ± 0.54 †, ‡, §	2.28 †, ‡, §	0.03 †, ‡, §	0.11 †, ‡	46.32 †, ‡, §
3DPQ-5	0.81 ± 0.43 †, ‡, §	74.41 ± 0.46 †, ‡, §	2.04 †	0.08 †, ‡, §	0.18 †, ‡	41.80 †, ‡, §
3DPQ-6	0.84 ± 0.11 †, ‡, §	86.56 ± 0.33 †, ‡, §	2.03 †	0.01 †, ‡, §	0.19 †	48.63 †, ‡, §
3DPQ-7	0.64 ± 0.13 †, ‡, §	72.34 ± 0.17 †, ‡, §	2.14 †, ‡	0.09 †, ‡, §	0.14 †, ‡	40.64 †, ‡, §
3DPQ-8	0.81 ± 0.14 †, ‡, §	72.35 ± 0.78 †, ‡, §	2.04 †	0.09 †, ‡, §	0.18 †, ‡	40.65 †, ‡, §
3DPQ-9	0.45 ± 0.14 †, ‡, §	83.56 ± 0.46 †, ‡, §	2.30 †, ‡, §	0.03 †, ‡, §	0.10 †, ‡	46.94 †, ‡, §
3DPQ-10	0.77 ± 0.14 †, ‡, §	79.54 ± 0.76 †, ‡, §	2.06 †	0.05 †, ‡, §	0.17 †, ‡	44.69 †, ‡, §
3DPQ-11	0.70 ± 0.33 †, ‡, §	76.52 ± 0.48 †, ‡, §	2.10 †	0.07 †, ‡, §	0.16 †, ‡	42.99 †, ‡, §
3DPQ-12	0.40 ± 0.43 †, ‡, §	89.45 ± 0.31 †, ‡, §	2.35 †, ‡, §	0.00 †, ‡, §	0.09 †, ‡, §	50.25 †, ‡, §
E_2^h	0.88 ± 0.24 †, §	0.88 ± 0.32 †, §	2.00	2.00 †, §	0.20 †, §	0.49 †, §
4-OHT . ⁱ	1.13 ± 0.24 †, §	3.62 ± 0.43 †, §	1.90 §	1.39 †	0.25 †, §	2.03 †, §
Ral . ^j	0.73 ± 0.35 †, ‡	3.39 ± 0.16 †, ‡	2.09 †	1.42 †	0.16 †, ‡	1.90 †, ‡
Control . ^k	NA ^l	NA	NA	NA	NA	NA

^a Concentration that antagonizes the 50% of $\text{ER}\alpha$ signaling activity; ^b Concentration that antagonizes (inhibits) the 50% of $\text{ER}\beta$ signaling activity; ^c Logarithmic value of the percentage of relative binding affinity toward the $\text{ER}\alpha$; ^d Logarithmic value of the percentage of relative binding affinity toward the $\text{ER}\beta$ (for both ^c values and ^d values relative binding affinity (RBA) values where calculated related to estradiol with an affinity of 100%, $\log\text{RBA}$ values higher than 0 refer to strong binders, $\log\text{RBA}$ values between -2 and 0 refer to moderate binders, $\log\text{RBA}$ values below -2 refer to weak binders); ^e Calculated antagonistic (i.e., inhibitory) constants against $\text{ER}\alpha$; ^f Calculated antagonistic (i.e., inhibitory) constants against $\text{ER}\beta$; ^g Results are presented as mean value \pm standard deviation; ^h **17 β -estradiol**; ⁱ **4-hydroxytamoxifen**; ^j **Raloxifene**; ^k No ligand (0.9% NaCl). ^l Not available. * $p < 0.05$ when compared with control group; † $p < 0.05$ when compared with E_2 ; ‡ $p < 0.05$ when compared with **4-OHT**; § $p < 0.05$ when compared with **Ral**.

The substitution of the bulky heterocycle, bearing an HBD, with a sulphonyl group, like as in the SERM **3DPQ-4** (Table 7, Supplementary Materials Figure S191D, Figure 7D, 1.57-fold stronger binder than **Ral**), lowered the potency by only a low nM fraction relative to **3DPQ-12**, despite the sulphonyl group forming a weak HB with Asp351 (the $d_{\text{HB}} = 3.347 \text{ \AA}$). However, the sulphonyl group replacement with either *N,N*-dimethyl, or *N*-methyl ones, within **3DPQ-2** (Supplementary Materials Figure S191E, Table 7, Figure 7E) and **3DPQ-1** (Supplementary Materials Figure S191F, Table 7, Figure 7F) as SERMs (HB lengths with Asp351 of 3.122 and 3.083 \AA , respectively), led to a potency decrease (compounds were still 1.37-fold to 1.30-fold more potent than **Ral**, respectively).

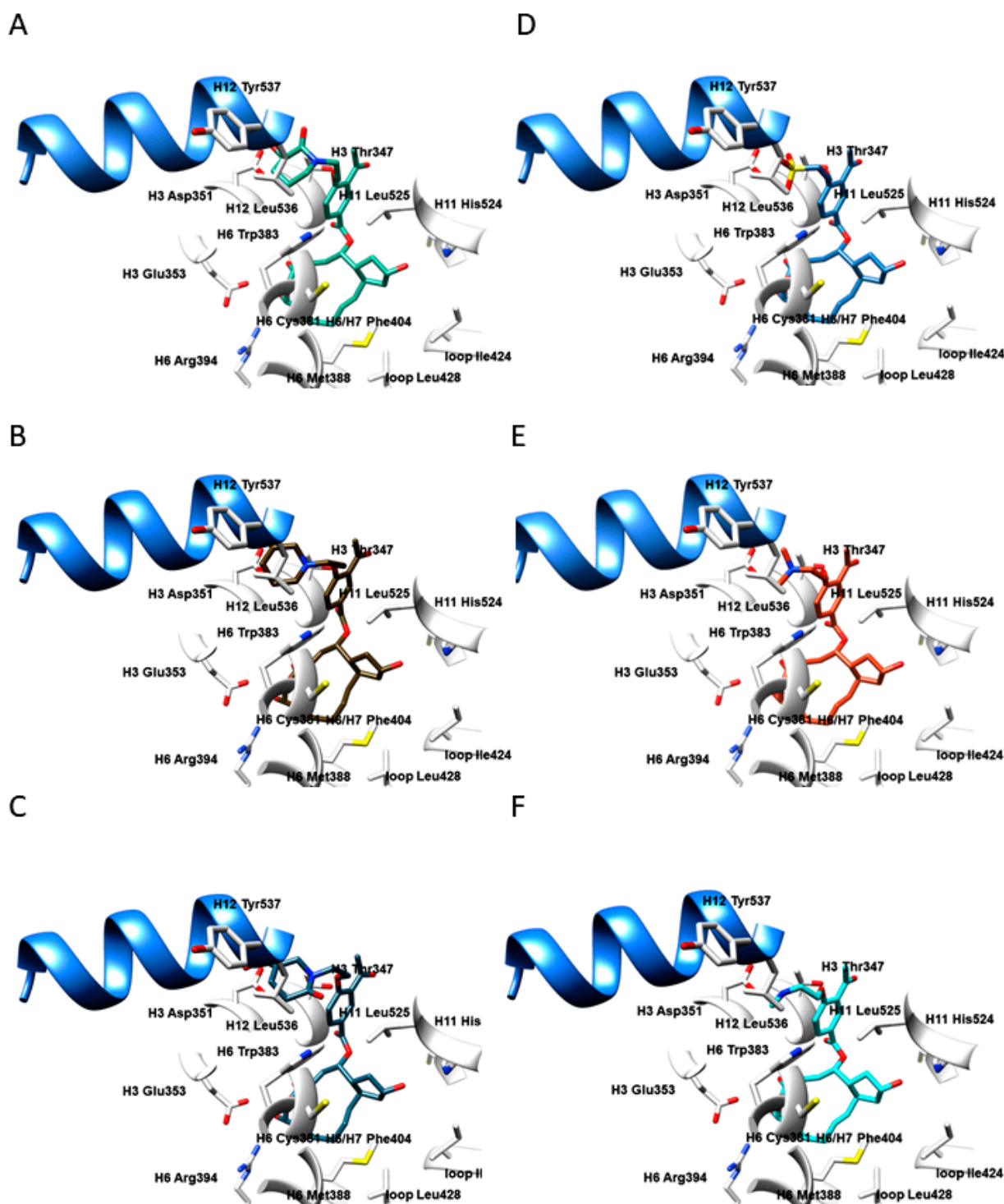


Figure 7. The bioactive conformations of 3DPQ-12 (A); 3DPQ-3 (B); 3DPQ-9 (C); 3DPQ-4 (D); 3DPQ-2 (E); 3DPQ-1 (F) within the ER α active site. Amino acid residues are depicted in white, H12 helix is presented in cornflower blue ribbon.

SERMs like 3DPQ-7 (Table 7, Supplementary Materials Figures S192A and S195A, 1.16-fold more potent than *Ral*) and 3DPQ-11 (Table 7, Supplementary Materials Figures S192B and S195B, 1.06-fold more potent than *Ral*) formed via 1,2-dihydroisoquinoline and 1-(2-chloroethyl)pyrrolidine scaffolds hydrophobic interactions with the Leu536 isobutyl group and weaker HBs with Asp351 ($d_{\text{HBs}} = 3.922$ and 3.136 Å, respectively, thus lowering the potency) via the nitrogen atom. Furthermore, the piperidine (3DPQ-10, Table 7, Supplemen-

tary Materials Figures S192C and S195C, 1.45-fold more potent than 4-OHT), pyrrolidine-2,5-dione (3DPQ-5, Table 7, Supplementary Materials Figures S192D and 195D, 1.38-fold more potent than 4-OHT), decahydro-1,8-naphthyridine (3DPQ-8, Table 7, Supplementary Materials Figures S192E and 195E, 1.38-fold more potent than 4-OHT), and 6,7-dihydro-5H-pyrrolo [3,4-b]pyridine (3DPQ-6, Table 7, Supplementary Materials Figures S192F and 195F, 1.33-fold more potent than 4-OHT) reduced the potency due to their inability to form HBs with Asp351.

2.8. Synthesized Compounds Antiproliferative Activity against ER α (+)- and ER α (-)-Dependent Breast Cancer Cell Lines as Well as against ER α (+)-Dependent Endometrial Cancer Cell Lines

Synthesized compounds were evaluated as antiproliferative agents against MCF-7 (Table 8, Supplementary Materials Figures S196 and S197), and MDA-MB-231 (Table 8, Supplementary Materials Figures S198 and S199) cells lines [130], respectively, as well as for the ability to induce ER α downregulation in MCF-7 cells (Table 8) [15,21,131,132] and to antagonize the progesterone receptor (PR) (Table 8) [126].

Table 8. Synthesized compound antiproliferative activity and selectivity index against hormone-dependent MCF-7, hormone-independent MDA-MB-231 breast cancer cell lines, normal MRC-5 human lung tissue fibroblasts cell lines, and Ishikawa endometrial adenocarcinoma cell lines, as well as the downregulation of ER α in MCF-7 and PR antagonism in MCF-7 cell lines.

Comp.	MCF-7 ^a (IC ₅₀ nM)	MDA-MB-231 ^b (IC ₅₀ nM)	SI ^c	MRC-5 ^d (IC ₅₀ nM)	MCF-7 DR ^e (IC ₅₀ nM)	PR MCF-7 ^f (IC ₅₀ nM)	Ishikawa ^g (IC ₅₀ nM)
3DPQ-1	0.76 ± 0.24 ^{h,†,§}	72.44 ± 0.32 ^{†,§}	95.31 ^{†,§}	>100	>100	>100	0.94 ± 0.36 ^{g,†,§}
3DPQ-2	0.73 ± 0.42 ^{†,§}	72.42 ± 0.47 ^{†,§}	99.20 ^{†,§}	>100	>100	>100	0.99 ± 0.35 [†]
3DPQ-3	0.61 ± 0.56 ^{†,§}	86.63 ± 0.68 ^{†,§}	142.02 ^{†,§}	>100	>100	>100	0.84 ± 0.74 ^{†,§}
3DPQ-4	0.64 ± 0.15 ^{†,§}	67.31 ± 0.34 ^{†,§}	105.17 ^{†,§}	>100	>100	>100	0.92 ± 0.43 ^{†,§}
3DPQ-5	1.02 ± 0.64 ^{†,§}	52.64 ± 0.69 ^{†,§}	51.61 ^{†,§}	>100	>100	>100	1.42 ± 0.32 ^{†,§}
3DPQ-6	1.14 ± 0.49 ^{†,§}	52.31 ± 0.46 ^{†,§}	45.89 ^{†,§}	>100	>100	>100	1.46 ± 0.43 ^{†,§}
3DPQ-7	0.78 ± 0.52 ^{†,§}	51.96 ± 0.68 ^{†,§}	66.61 ^{†,§}	>100	>100	>100	1.74 ± 0.43 ^{†,§}
3DPQ-8	1.06 ± 0.45 ^{†,§}	42.56 ± 0.35 ^{†,§}	40.15 ^{†,§}	>100	>100	>100	1.98 ± 0.32 ^{†,§}
3DPQ-9	0.62 ± 0.15 ^{†,§}	81.63 ± 0.42 ^{†,§}	131.66 ^{†,§}	>100	>100	>100	0.89 ± 0.24 ^{†,§}
3DPQ-10	0.97 ± 0.34 ^{†,§}	41.97 ± 0.32 ^{†,§}	42.27 ^{†,§}	>100	>100	>100	1.55 ± 0.42 ^{†,§}
3DPQ-11	0.81 ± 0.22 ^{†,§}	67.12 ± 0.54 ^{†,§}	82.86 ^{†,§}	>100	>100	>100	1.37 ± 0.47 ^{†,§}
3DPQ-12	0.56 ± 0.11 ^{†,§}	82.84 ± 0.61 ^{†,§}	147.93 ^{†,§}	>100	>100	>100	0.77 ± 0.43 ^{†,§}
E ₂ ⁱ	N ^m	NA	NA	NA	NA	NA	NA
4-OHT ^j	1.19 ± 0.57 [§]	37.10 ± 0.45 [§]	31.18 [§]	>10	>100	>100	1.29 ± 0.43 [§]
Ral. ^k	0.90 ± 0.19 [†]	93.41 ± 0.48 [†]	103.97 [†]	>10	>100	>100	0.97 ± 0.35 [†]
Control ^l	NA	NA	NA	NA	NA	NA	NA

^a Concentration that prevents the growth of 50% of MCF-7 cell lines; ^b Concentration that prevents the growth of 50% of MDA-MB-231 cell lines; ^c Selectivity index toward the cell line: [IC₅₀(MDA-MB-231)]/[IC₅₀(MCF-7)] for the antiproliferative effect of both designed compounds and reference compounds; ^d Concentration that prevents the growth of 50% of MRC-5 cell lines (human lung fibroblast cell lines, as a neutral control); ^e ER α downregulation measured in MCF-7 cell lines; ^f Progesterone receptor was measured as a biomarker for ER α antagonism in MCF-7 cell lines; ^g Concentration that prevents the growth of 50% of Ishikawa cell lines; ^h Results are presented as mean value ± standard deviation; ⁱ 17 β -estradiol; ^j 4-hydroxytamoxifen; ^k Raloxifene; ^l 0.9%NaCl; ^m Not available. * $p < 0.05$ when compared with control group. † $p < 0.05$ when compared with 4-OHT; § $p < 0.05$ when compared with Ral.

Compounds-proposed bioactive conformations anticipated a SERM-like profile, which was experimentally confirmed as they induced no ER α degradation, at the same time exerting no antagonism against PR (Table 8) [125]. Therefore, the further focus was on the antiproliferative activity, where even eight derivatives showed antiproliferation against MCF-7 better or comparable to Ral (Table 8). 3DPQ-12 (Table 8, Supplementary Materials Figure S196A) was the most potent MCF-7 cell growth inhibitor with an IC₅₀ value equal to 560 pM and a selectivity index (SI) relative to MDA-MB-231 cell lines of 147.93. Similar antiproliferation profiles were also exerted by 3DPQ-3 (Table 8, Supplementary Materials

Figure S196B, potency 1.11-fold lower than **3DPQ-12** but 1.43-fold higher than **Ral**, SI equal to 131.66) and **3DPQ-9** (Table 8, Supplementary Materials Figure S196C, potency 1.09-fold lower than **3DPQ-12** but 1.46-fold more potent than **Ral**, SI equal to 142.02).

Comparably with the latter two, **3DPQ-4** (Table 8, Supplementary Materials Figure S196D) had an antiproliferative potency 1.14-fold lower than **3DPQ-12** and 1.39-fold higher than **Ral**, with an SI of 105.17. The **3DPQ-2** (Table 8, Supplementary Materials Figure S196E, 1.21-fold more potent than **Ral**), **3DPQ-1** (Table 8, Supplementary Materials Figure S196F, 1.17-fold more potent than **Ral**), **3DPQ-7** (Table 8, Supplementary Materials Figure S197A, 1.14-fold more potent than **Ral**), and **3DPQ-11** (Table 8, Supplementary Materials Figure S197B, 1.10-fold more potent than **Ral**) showed antiproliferative potency ranging from 730 and 810 pM, but with lower SIs.

As SERMs profile is often associated with the stimulation of endometrial cell proliferation and an increase in the incidence of endometrial cancer (EC) [130], the herein compounds were therefore evaluated against Ishikawa endometrial adenocarcinoma cells (Table 8, Supplementary Material Figures S200 and S201). At this stage of evaluation, the herein SERMs significantly inhibited Ishikawa cell lines growth. However, future experimental elaboration, currently beyond the authors' experimental facilities, is required to confirm compounds' promising profiles in terms of no EC induction [130].

2.9. The Impact of Targeted ER α Antagonists on the MCF-7 Cells Signaling

The exerted antiproliferation against MCF-7 cell lines was further inspected for the inner mechanisms of action. **BFA** is known for inducing the endoplasmic reticulum stress within the MCF-7 cell lines, as well as for increasing the expression of p53, a major BC suppressor [132]. Nonetheless, ER α binds to p53, resulting in the inhibition of transcriptional regulation by p53, p53-mediated cell cycle arrest, and apoptosis [133], raising the question of whether the ER α antagonists herein described could have also inhibited MCF-7 cells' growth by decreasing the ER α recruitment and by stimulating the p53's transactivation function. To investigate this hypothesis, the conventional and sequential site-specific ChIP assays were employed to reveal the mechanisms by which the **3DPQ-1** to **3DPQ-12** antagonized ER α influenced the p53-mediated transcriptional activation of the p21 gene (a prototypic p53-target gene) [133]. Experimentally, all the compounds except **3DPQ-5**, **3DPQ-6**, and **3DPQ-8** have been re-administered in 0.1 and 1 nM to MCF-7 cells (i.e., two concentrations encircling the IC₅₀ values against MCF-7 cells, Table 8); for the marked compounds, the concentrations were 1 and 10 nM.

Upon the addition of primers specific to the p53-binding site of the p21 promoter, the chromatin was immunoprecipitated with the anti-p53 antibody and re-immunoprecipitated with the anti-ER α antibody, enabling the conclusion that the p53 expression occurred after the ER α has been antagonized by compounds (Figure 8A). The final round of re-immunoprecipitation was performed with NCoR and SMRT corepressors, guided by the premise that **3DPQ-1** to **3DPQ-12** as antiestrogens could promote their binding to ER α , followed by the recruitment of HDACs and leading to transcriptional repression [134,135]. Nonetheless, as NCoR, SMRT, and HDAC1 had been not recruited to the p21 promoter when ER α was knocked down (Figure 8B), ER α -**3DPQ-1** to ER α -**3DPQ-12** complexes, conversely to ER α , stimulated the p53-mediated transcriptional activation without recruiting the distinct corepressors.

Furthermore, the quantitative ChIP (qChIP) analysis measured the strength of **3DPQ-1** to **3DPQ-12** to affect the ER α 's ability to bind to p53. Contrary to E₂, **3DPQ-1** to **3DPQ-12** disrupted the receptor's interaction with the p21 promoter (Figure 8A) and stimulated the p53 transcriptional activity. The highest rate of p53 promoter activity was induced upon the **3DPQ-12**, **3DPQ-3**, and **3DPQ-9** administration, 0.65-fold and 0.55-fold, 0.68-fold and 0.61-fold, as well as 0.68-fold and 0.66-fold higher than the one provoked by **Ral** in lower and higher concentrations, respectively (Figure 8B). The **3DPQ-4** was similarly potent to **3DPQ-9**, exerting 0.70-fold and 0.68-fold higher potency than **Ral**, respectively, whereas **3DPQ-2** and **3DPQ-1** exerted the matching potency, 0.733-fold and 0.66-fold higher than

Ral (Figure 8A). Conclusively, as ER α and SERMs, 3DPQ-1 to 3DPQ-12 have indeed decreased ER α recruitment and stimulated the p53 (p21) pathway, as another way of preventing the growth of MCF-7 cells.

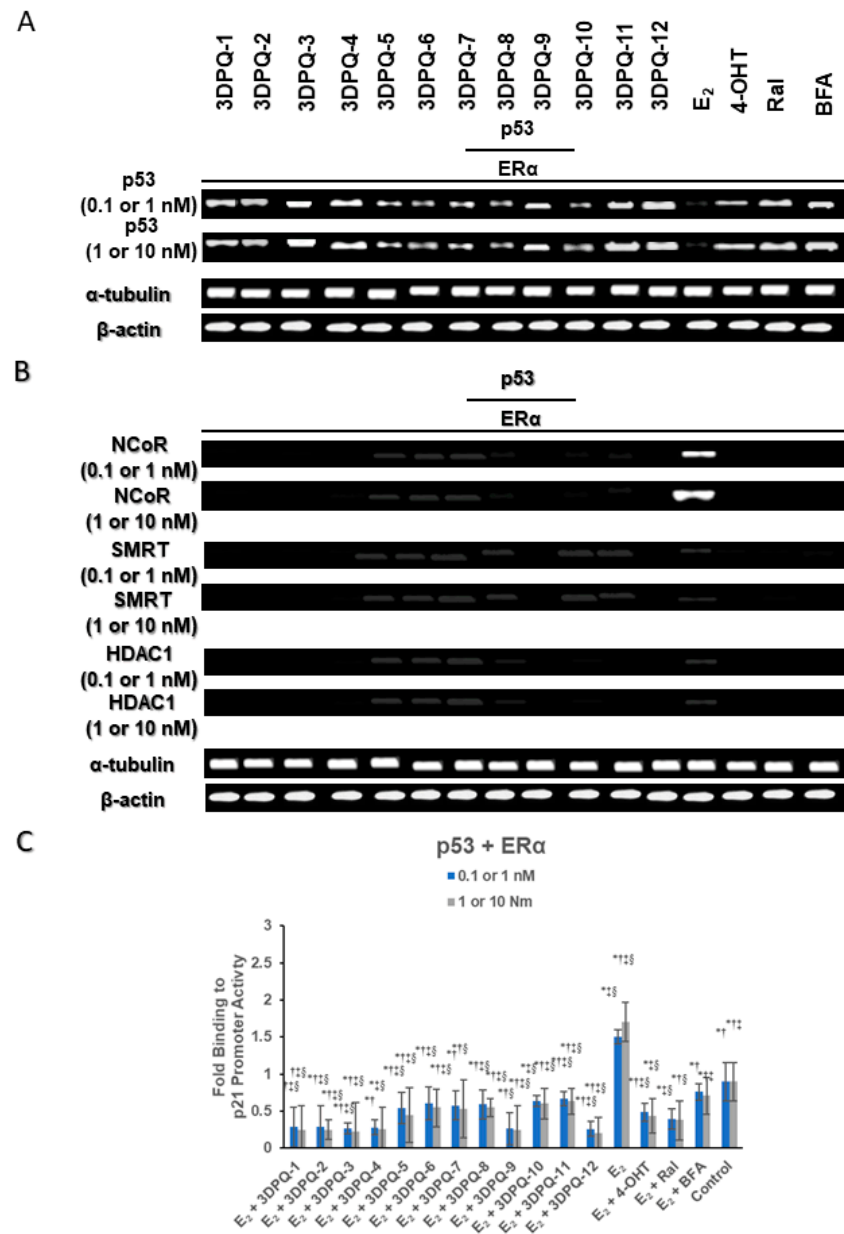


Figure 8. ER α recruits transcriptional corepressors to repress p53-mediated transcriptional activation. (A) ChIP and sequential ChIP assays were performed on MCF-7 cells saturated with 3DPQ-1 to 3DPQ-12 in concentrations of 0.1 and 1 nM (for 3DPQ-5, 3DPQ-6, and 3DPQ-8 the concentrations were 1 and 10 nM) with primers specific to the p53-binding site of the p21 promoter. The primary ChIP was performed with anti-p53 antibody, and the immunoprecipitate was subjected to a second ChIP with anti-ER α antibody; (B) The immunoprecipitate from the ER α ChIP was then subjected to the third ChIP with antibodies against NCoR, SMRT, and HDAC1 antibodies; (C) qChIP was performed to analyze the ER α -p53 interaction on the p21 promoter in MCF-7 cells saturated with 3DPQ-1 to 3DPQ-12. Cells were grown in media with dextran-coated charcoal-treated FBS for 4 d and treated with E₂ (1 and 10 nM) with or without 3DPQ-1 to 3DPQ-12 for 3 h. * $p < 0.05$ when compared with control group; † $p < 0.05$ when compared with E₂; ‡ $p < 0.05$ when compared with 4-OHT; § $p < 0.05$ when compared with Ral.

2.10. Effects of Synthesized Compounds on Cytotoxicity and Cell Cycle Distribution of MCF-7 Cell Lines

The above data encouraged further analysis of the cell cycle of MCF-7 cells treated by **3DPQ-1** to **3DPQ-12** (Table 9, Supplementary Material Figures S202–S213) [130], administered at the same concentrations used for the cell signaling assay. Thus, compounds induced the MCF-7 cells' arrest in the G₀/G₁ phase, i.e., the phase in between the non-division, post mitosis (viz., G₀), and DNA replication (viz., G₁). The G₀/G₁ phase arrest was accompanied by a decrease in the S phase, suggesting that compounds stopped the MCF-7 proliferation before the DNA replication induced by the transcriptional machinery. The results agreed with previous findings that SERMs block MCF-7 cell cycle progression in G₀/G₁ [136]. It is worth emphasizing that for all the compounds, applied in both concentrations, the contribution of the G₀/G₁ phase to the MCF-7 cells' arrest was higher than 70%.

Table 9. Effects of synthesized compounds on the MCF-7 cell cycle.

Comp. Stage	Cell Cycle (%)					
	G ₀ /G ₁ ^{a,b}		S ^c		G ₂ /M ^{d,e}	
Conc. (nM)	0.1 (1) ^f	1 (10)	0.1 (1) ^f	1 (10)	0.1 (1) ^f	1 (10)
3DPQ-1	72.62 ± 2.47 ^{*,†,‡,§}	75.08 ± 2.13 ^{*,†,‡,§}	9.98 ± 1.65 ^{*,†,‡,§}	10.69 ± 1.42 ^{*,†,‡,§}	17.40 ± 3.63 ^{*,†,‡,§}	14.24 ± 2.54 ^{*,†,‡,§}
3DPQ-2	73.64 ± 5.32 ^{*,†,‡,§}	76.10 ± 1.43 ^{*,†,‡,§}	11.88 ± 0.87 ^{*,†,‡,§}	12.59 ± 1.57 ^{*,†,‡,§}	14.48 ± 2.54 ^{*,†,‡,§}	11.32 ± 3.25 ^{*,†,‡,§}
3DPQ-3	72.99 ± 1.32 ^{*,†,‡,§}	75.45 ± 1.53 ^{*,†,‡,§}	8.98 ± 1.64 ^{*,†,‡,§}	9.69 ± 0.94 ^{*,†,‡,§}	18.03 ± 1.65 ^{*,†,‡,§}	14.87 ± 2.43 ^{*,†,‡,§}
3DPQ-4	77.78 ± 3.54 ^{*,†,‡,§}	80.24 ± 2.53 ^{*,†,‡,§}	7.20 ± 2.88 ^{*,†,‡,§}	7.91 ± 0.154 ^{*,†,‡,§}	15.02 ± 4.23 ^{*,†,‡,§}	11.86 ± 3.43 ^{*,†,‡,§}
3DPQ-5	71.78 ± 0.67 ^{*,†,‡,§}	74.24 ± 2.15 ^{*,†,‡,§}	9.21 ± 1.95 ^{*,†,‡,§}	9.92 ± 0.76 ^{*,†,‡,§}	19.01 ± 3.55 ^{*,†,‡,§}	15.85 ± 4.43 ^{*,†,‡,§}
3DPQ-6	70.52 ± 1.53 ^{*,†,‡,§}	71.98 ± 2.44 ^{*,†,‡,§}	13.27 ± 2.64 ^{*,†,‡,§}	13.98 ± 1.33 ^{*,†,‡,§}	16.21 ± 3.25 ^{*,†,‡,§}	14.05 ± 2.43 ^{*,†,‡,§}
3DPQ-7	73.25 ± 2.54 ^{*,†,‡,§}	75.71 ± 1.43 ^{*,†,‡,§}	14.06 ± 1.58 ^{*,†,‡,§}	14.77 ± 1.46 ^{*,†,‡,§}	12.69 ± 2.64 ^{*,†,‡,§}	9.53 ± 3.54 ^{*,†,‡,§}
3DPQ-8	72.39 ± 1.43 ^{*,†,‡,§}	74.85 ± 2.54 ^{*,†,‡,§}	12.50 ± 1.22 ^{*,†,‡,§}	13.21 ± 2.15 ^{*,†,‡,§}	15.11 ± 2.56 ^{*,†,‡,§}	11.95 ± 2.45 ^{*,†,‡,§}
3DPQ-9	71.47 ± 0.99 ^{*,†,‡,§}	75.93 ± 1.52 ^{*,†,‡,§}	12.97 ± 1.65 ^{*,†,‡,§}	13.68 ± 1.74 ^{*,†,‡,§}	15.56 ± 2.65 ^{*,†,‡,§}	10.40 ± 3.54 ^{*,†,‡,§}
3DPQ-10	71.96 ± 1.43 ^{*,†,‡,§}	74.42 ± 2.12 ^{*,†,‡,§}	11.96 ± 2.41 ^{*,†,‡,§}	12.67 ± 2.46 ^{*,†,‡,§}	16.08 ± 1.56 ^{*,†,‡,§}	12.92 ± 4.32 ^{*,†,‡,§}
3DPQ-11	72.53 ± 0.47 ^{*,†,‡,§}	74.99 ± 2.54 ^{*,†,‡,§}	13.31 ± 1.66 ^{*,†,‡,§}	14.02 ± 1.43 ^{*,†,‡,§}	14.16 ± 2.13 ^{*,†,‡,§}	11.00 ± 3.43 ^{*,†,‡,§}
3DPQ-12	77.83 ± 0.92 ^{*,†,‡,§}	80.29 ± 1.24 ^{*,†,‡,§}	16.96 ± 1.23 ^{*,†,‡,§}	17.67 ± 1.32 ^{*,†,‡,§}	5.21 ± 2.54 ^{*,†,‡,§}	2.05 ± 1.43 ^{*,†,‡,§}
E₂^g	17.34 ± 0.35 ^{*,†,‡,§}	25.34 ± 0.36 ^{*,†,‡,§}	28.15 ± 0.52 ^{*,†,‡,§}	29.52 ± 0.46 ^{*,†,‡,§}	54.51 ± 0.57 ^{*,†,‡,§}	45.14 ± 0.33 ^{*,†,‡,§}
4-OTH^h	57.22 ± 0.37 ^{*,†,‡,§}	63.26 ± 0.41 ^{*,†,‡,§}	18.76 ± 0.41 ^{*,†,‡,§}	21.14 ± 0.25 ^{*,†,‡,§}	24.02 ± 0.53 ^{*,†,‡,§}	15.60 ± 0.15 ^{*,†,‡,§}
Ral.ⁱ	59.14 ± 0.54 ^{*,†,‡,§}	66.52 ± 0.56 ^{*,†,‡,§}	15.83 ± 0.53 ^{*,†,‡,§}	16.37 ± 0.46 ^{*,†,‡,§}	25.03 ± 0.35 ^{*,†,‡,§}	17.11 ± 0.46 ^{*,†,‡,§}
Control^j	32.21 ± 0.45		34.97 ± 0.53		32.82 ± 0.35	

^a Cell resting states: G₀—a cell has left the cycle and has stopped dividing; ^b Cell interphase (i.e., synthesis) state: G₁—cells size increase (preparation for DNA synthesis); ^c Cell interphase (i.e., synthesis) state: S DNA replication; ^d Cell interphase (i.e., synthesis) state: G₂—the gap between DNA synthesis and mitosis, in which the cell continues to grow; ^e Cell division states: M cell growth stops, division occurs; ^f The compounds concentration in nM administered to MCF-7 cells (all the compounds except **3DPQ-5**, **3DPQ-6**, and **3DPQ-8** have been re-administered in concentrations of 0.1 and 1 nM; for the marked compounds, the concentrations were 1 and 10 nM; Values: mean ± standard deviation. ^g **17β-estradiol**; ^h **4-hydroxytamoxifen**; ⁱ **raloxifene**; ^j 0.9% NaCl. * $p < 0.05$ when compared with control group; [†] $p < 0.05$ when compared with E₂; [‡] $p < 0.05$ when compared with 4-OTH; [§] $p < 0.05$ when compared with Ral.

The distribution of **3DPQ-12** (Table 9, Supplementary Material Figures S202A,E), and **3DPQ-4** (Table 9, Supplementary Material Figures S205A,E) within the cell cycle mostly affected the cells' proliferation, reaching 77 to 80% of the contribution of the G₀/G₁ phase upon administering either 0.1 or 1 nM of the compound, respectively. On the other hand, **3DPQ-3** (Table 9, Supplementary Material Figures S203A,E), **3DPQ-9** (Table 9, Supplementary Material Figures S204A,E), **3DPQ-2** (Table 9, Supplementary Material Figures S206A,E), and **3DPQ-1** (Table 9, Supplementary Material Figures S207A,E) blocked the MCF-7 cycle in the initial phase between 71 and 76%. The cell cycle arrest in the G₀/G₁ phase may be a key mechanism by which targeted antiproliferative agents inhibit MCF-7 cell proliferation.

2.11. Prediction of ADMETox Properties for the Compounds

Before the in vivo examination, ADMETox properties [137] were predicted in silico to assess the safety of the compounds as drug-like compounds (Table 10).

Table 10. In silico physicochemical and pharmacokinetic properties of synthesized compounds.

Comp.	mol_MWT ^a	donorHB ^b	acceptHB ^c	QPlogPo/w ^d	PSA ^e	RO5 ^f	QPlogKhsa ^g	QPlogHERG ^h	QPPCaco ⁱ
3DPQ-1	501.243	3	9	2.11	133.084	2	−0.571	−5.759	26.396
3DPQ-2	515.254	2	9	2.49	124.532	1	−0.529	−5.242	27.138
3DPQ-3	597.263	3	11	2.29	131.324	3	−0.539	−5.354	31.352
3DPQ-4	552.175	3	11	1.43	136.387	3	−0.645	−5.367	25.872
3DPQ-5	569.234	2	11	1.45	160.686	3	−0.934	−4.029	26.464
3DPQ-6	590.261	2	10	3.01	154.432	2	0.005	−4.903	22.432
3DPQ-7	601.272	2	9	4.33	122.038	1	0.198	−5.836	34.075
3DPQ-8	610.336	3	10	3.51	133.649	2	0.191	−4.976	165.259
3DPQ-9	611.243	3	12	1.39	140.653	3	−0.562	−5.321	27.621
3DPQ-10	555.286	2	9	3.32	143.543	2	0.135	−4.324	132.594
3DPQ-11	541.276	2	9	2.81	143.653	2	0.162	−4.321	135.594
3DPQ-12	585.243	3	11	1.58	140.795	3	−0.900	−5.239	26.295
E ₂ ^s	278.434	2	3	2.487	47.727	0	0.214	−1.994	1322.153
4-OTH. ^t	407.679	1	5	4.201	36.102	0	0.669	−3.909	669.539
Ral ^u	495.759	3	9	2.381	73.257	0	0.173	−3.648	130.539
	QPPMDCK ^j	QPlogBB ^k	A ^l	B ^m	C ⁿ	D ^o	E ^p	F ^q	G ^r
3DPQ-1	26.435	−1.964	−	−	−	−	−	−	−
3DPQ-2	31.095	−1.892	−	−	−	−	−	−	−
3DPQ-3	34.542	−2.963	−	−	−	−	−	−	−
3DPQ-4	31.921	−2.735	−	−	−	−	−	−	−
3DPQ-5	32.351	−2.029	−	−	−	−	−	−	+
3DPQ-6	23.658	−2.432	−	−	−	−	+	−	+
3DPQ-7	14.190	−3.977	−	−	+	+	+	−	+
3DPQ-8	70.677	−3.237	−	−	−	−	+	−	+
3DPQ-9	36.284	−2.876	−	−	−	−	−	−	+
3DPQ-10	16.325	−3.321	−	−	+	−	−	−	−
3DPQ-11	18.362	−3.431	−	−	+	−	−	−	−
3DPQ-12	32.285	−2.682	−	−	−	−	−	−	+
E ₂ ^s	669.023	−0.209	−	−	−	−	−	−	−
4-OTH. ^t	354.743	−0.136	−	−	−	−	−	−	−
Ral ^u	88.081	−0.582	−	−	−	−	−	−	−

^a Molecular weight (range:130.0–725.0); ^b Number of hydrogen bond donors (range: 0.0–6.0); ^c Number of hydrogen bond acceptors (range: 2.0–20.0); ^d Predicted *n*-octanol/water partition coefficient (Range: −2.0–6.5); ^e Van der Waals surface area (Range: 7.0 to 200.0); ^f Lipinski's rule of five violations number (range: maximum is 4); ^g Prediction of human serum albumin binding (Range: −1.5 to +1.5); ^h Predicted IC₅₀ for HERG K⁺ channels blockage (optimal: −5); ⁱ Predicted Caco-2 cell permeability in nm/sec (a gut–blood barrier model; <25 poor, >500 great); ^j Predicted MDCK cell permeability in nm/sec (a blood–brain barrier model; <25 poor, >500 great); ^k Predicted brain/blood partition coefficient (range: −3.0 to 1.2); ^l Carcinogenicity; ^m Eye corrosion; ⁿ Eye irritation; ^o Ames mutagenesis; ^p Hepatotoxicity; ^q PPAR gamma; ^r Androgen receptor binding; Active = (+), Inactive = (−); ^s 17β-estradiol; ^t 4-hydroxytamoxifen; ^u raloxifene.

Hence, considering the Lipinski rule of five (RO5) (molecular weight < 500 Da, *n*-octanol–water partition coefficient < 5, hydrogen bond donor ≤ 5, hydrogen bond acceptor ≤ 10, polar surface area between 40–130) [138], of all the examined compounds only 3DPQ-2 and 3DPQ-7 could be considered drug-like, as they violated one or fewer of the RO5 criteria.

However, as more compounds that do not obey all the RO5 rules still reach the market as commercial drugs [139], tentative attempts have been made to revise RO5 [140–143]. Therefore, the optimal physicochemical and pharmacokinetic properties are considered preferable to RO5 [137]. In that sense, the binding to human serum albumin (QPlogKhsa), the IC₅₀ values for the blockage of HERG K⁺ channels (QPlogHERG), the Caco-2 cell (i.e., the gut–blood barrier) permeability (QPPCaco), as well as the MDCK cell (i.e., the blood–brain barrier mimic) permeability (QPPMDCK), and the brain/blood partition coefficient (QPlogBB) were predicted by means of the Schrödinger's QikProp module [144]. Indeed, the 3DPQ-12, 3DPQ-3, 3DPQ-9, 3DPQ-4, 3DPQ-2, and 3DPQ-1, as the most promising compounds elaborated so-far, showed optimal QPlogKhsa, QPlogHERG, and QPPCaco, accompanied by satisfying values for QPPMDC and QPlogBB. The toxicological assessments of organ and genomics performed by virtue of the admetSAR 2.0 webserver (<http://lmmd.ecust.edu.cn/admetSar2>, accessed on 1 March 2022) [145], viz., carcinogenic-

ity, eye corrosion, eye irritation, Ames mutagenesis, micronuclear, hepatotoxicity androgen receptor binding, and PPAR- γ gamma, proved the safety of the leads.

2.12. *In Vivo* Anticancer Screening

Due to the observed data, **3DPQ-12**, **3DPQ-3**, **3DPQ-9**, **3DPQ-4**, **3DPQ-2**, and **3DPQ-1** were subjected to the *in vivo* screening to determine their impact on the mammary tumorigenesis (Table 11) [146].

Experimentally, the adult female Wistar rats were pretreated intraperitoneally (*i.p.*) with methyl nitrosourea (MNU) with a dose of 50 mg/kg of each rat's body weight (bwt) to induce the BC, after which the compounds herein described were administered *per os* in two doses, 5 and 50 mg/kg of bwt [81]. The compounds were evaluated employing latency period (i.e., the time passed between the rats being exposed to MNU and the BC detection), tumor burden (i.e., the number of cancer cells), and tumor volume.

Hence, **3DPQ-12**, **3DPQ-3**, and **3DPQ-9** induced the longest latency period, 12 to 15 weeks depending on the concentration applied, followed by its low burden and volume, overpowering the efficiency of **Ral** (Table 11). The **3DPQ-4** induced a latency period between 9 and 12 weeks. The remaining leads, **3DPQ-2** and **3DPQ-1**, were slightly less efficient tumor suppressants, with tumor latency between 7 to 12 weeks and more emphasized tumor burdens and volumes, but were still more potent than **Ral**. Of course, the safety of the compound during administration was confirmed with liver enzyme catalytic activities and redox status [147–155] (Supplementary Materials Tables S19 and S20), where no significant harm was detected.

Being orally administered to rats, **3DPQ-12**, **3DPQ-3**, **3DPQ-9**, **3DPQ-4**, **3DPQ-2**, and **3DPQ-1** exerted good pharmacokinetic profiles (Table 11) [74,156], with high affinity for plasma protein binding [157], relatively low *in vivo* clearances [158], and no damage to hepatocytes, which correlated with results concerning the low liver enzyme catalytic activities redox status (Supplementary Materials Tables S19 and S20). Overall good oral exposure was observed in all the leads alongside favorable bioavailability.

The impact of selected leads on BC tissue was registered after their administration to experimental animals with MNU-induced BC (Figures 9 and S211–S218) [159]. Thus, compared to the normal pathological finding of animals treated with saline, reflected in photomicrographs revealing lobuloalveolar unit (LaU) and cuboidal epithelial cells (CE) (Figure 9A), MNU provoked ductal mammary gland carcinoma and massive proliferation of neoplastic epithelial cells (EC) (Figure 9B), changes found within the terminal ductal-lobular unit, that formed discrete clusters with duct-like morphology. In contrast to this, the administered leads were harmless in both concentrations, neutralizing the MNU-induced changes, judging by the lobuloalveolar units and cuboidal epithelial cells found (Figures 9C,D and S214–S218). These compounds were safer than **4-OHT**, which caused severe necrosis (NEC) (Figure 9E,F), and **Ral**, which caused extralobular ducts (ED) (Figure 9G,H).

Table 11. Effects of synthesized compounds on mammary tumorigenesis.

Comp.	Dose (mg/kg)	log D _{7,4} ^a	Tumor Latency (week)	Tumor Burden (week)	Tumor Volume (mm ³)	Rat PPB ^b (%free)	Rat CL ^c in vivo	BIO ^d	MFD ^e (5 days) (mg/kg)	WL after MFD ^f (day 1, mg) ^g (day 5, mg) ^h
3DPQ-1	5	1.94 ‡	9 *	3.38 ± 0.31 ^{i,*‡}	1.09 ± 0.23 ^{*‡‡}	1.33 ‡	60 ‡	91	1000	310.34 ± 0.34 ⁱ
	50		12 ^{*‡}	2.04 ± 0.35 ^{*‡§±}	0.68 ± 0.35 ^{*‡§±}	1.22 §±	69 §±	94		300.23 ± 0.62
3DPQ-2	5	1.99 ‡	9 *	3.34 ± 0.57 ^{*‡}	0.96 ± 0.41 ^{*‡}	1.15 ‡	59 ‡	92	1000	305.03 ± 0.66
	50		12 ^{*‡}	1.98 ± 0.45 ^{*‡§±}	0.69 ± 0.23 ^{*‡§±}	1.24 §±	64 §±	94		300.43 ± 0.65
3DPQ-3	5	2.07 ‡	12 ^{*‡‡}	2.18 ± 0.69 ^{*‡‡}	0.78 ± 0.43 ^{*‡‡}	1.34 ‡	66 ‡	90	1000	320.45 ± 0.62
	50		15 ^{*‡§}	1.16 ± 0.64 ^{*‡§±}	0.66 ± 0.21 ^{*‡§±}	1.47 §±	71 §±	93		300.31 ± 0.52
3DPQ-4	5	1.88 ‡	10 ^{*‡}	2.39 ± 0.56 ^{*‡‡}	0.98 ± 0.31 ^{*‡‡}	1.23 ‡	64 ‡	90	1000	320.73 ± 0.36
	50		14 ^{*‡}	1.33 ± 0.15 ^{*‡§±}	0.41 ± 0.23 ^{*‡§±}	1.51 §±	76 §±	93		305.56 ± 0.68
3DPQ-9	5	2.02 ‡	12 ^{*‡‡}	2.28 ± 0.47 ^{*‡‡}	0.77 ± 0.32 ^{*‡‡}	1.28 ‡	62 ‡	94 ‡	1000	315.54 ± 0.65
	50		15 ^{*‡§}	1.14 ± 0.65 ^{*‡§±}	0.40 ± 0.43 ^{*‡§±}	1.31 §±	78 §±	97		310.33 ± 0.95
3DPQ-12	5	2.06 ‡	12 ^{*‡‡}	2.24 ± 0.54 ^{*‡‡}	0.67 ± 0.22 ^{*‡‡}	1.24 ‡	63 ‡	93 ‡	1000	305.06 ± 0.94
	50		15 ^{*‡§}	0.94 ± 0.35 ^{*‡§±}	0.34 ± 0.11 ^{*‡§±}	1.31 §±	71 §±	96		299.56 ± 0.45
4-OTH ^j	5	3.64	7 *	3.36 ± 0.38 ^{*‡}	1.88 ± 0.35 ^{*‡}	1.85	35	88	1000	305.84 ± 0.59
	50		10 ^{*‡}	3.22 ± 0.21 ^{*‡±}	1.35 ± 0.63 ^{*‡±}	2.52 ±	42	94		297.65 ± 0.39
Ral ^k	5	2.39 ‡	8 *	3.11 ± 0.47 ^{*‡‡}	1.67 ± 0.31 ^{*‡‡}	1.85	36	93 ‡	1000	310.54 ± 0.45
	50		13 ^{*‡}	2.91 ± 0.22 ^{*‡§}	1.41 ± 0.54 ^{*‡§}	1.90 §	42	96		300.54 ± 0.48
MNU ^l	50	NA ^o	5 ^{*‡‡§ ±}	4.55 ± 0.15 ^{*‡§ ±}	4.48 ± 0.54	NA	NA	NA	100	305.44 ± 0.62
C ^m	NA	NA	0 ^{‡‡§ ±}	0 ^{‡‡§ ±}	0 ^{‡‡§ ±}	NA	NA	NA	NA	210.54 ± 0.29
Placebo ⁿ	NA	NA	NA	NA	NA	NA	NA	NA	NA	300.54 ± 0.63
		NA	NA	NA	NA	NA	NA	NA	NA	325.43 ± 0.29

^a The average lipophilicity from the concentration range 5, 10, 20, 30, 40, and 50 mg/kg of bwt measured using shake-flask methodology; ^b Plasma protein binding (PPB) at 37 °C; ^c Intrinsic clearance in vivo; ^d Bioavailability of compound; ^e Maximum-tolerated-dose obtained after the 5-days per os administration in the concentration of 5, 50, 100, 500, and 1000 mg/kg bwt; ^f The effect of the orally administered compound at maximum-tolerated-dose; ^g The effect of the orally administered compound at maximum-feasible-dose on the body weight at day 1, showing the average body weight (mg) in placebo/control and the compound-treated rats; ^h The effect of the orally administered compound at maximum-feasible-dose on the bodyweight 5 days after starting treatment at the time of sacrifice, showing the average body weight (mg) in placebo/control and the compound-treated rats; ⁱ Results are presented as mean value ± standard deviation; ^j 4-hydroxytamoxifen; ^k Raloxifene; ^l Methyl nitrosourea; ^m 0.9% NaCl; ⁿ Vehicle; carboxymethylcellulose; ^o Not available. * $p < 0.05$ when compared with control group; ‡ $p < 0.05$ when compared with MNU in concentration of 50 mg/kg; ‡ $p < 0.05$ when compared with 4-OTH in concentration of 5 mg/kg; § $p < 0.05$ when compared with 4-OTH in concentration of 50 mg/kg; || $p < 0.05$ when compared with Ral in concentration of 5 mg/kg; ± $p < 0.05$ when compared with Ral in concentration of 50 mg/kg.

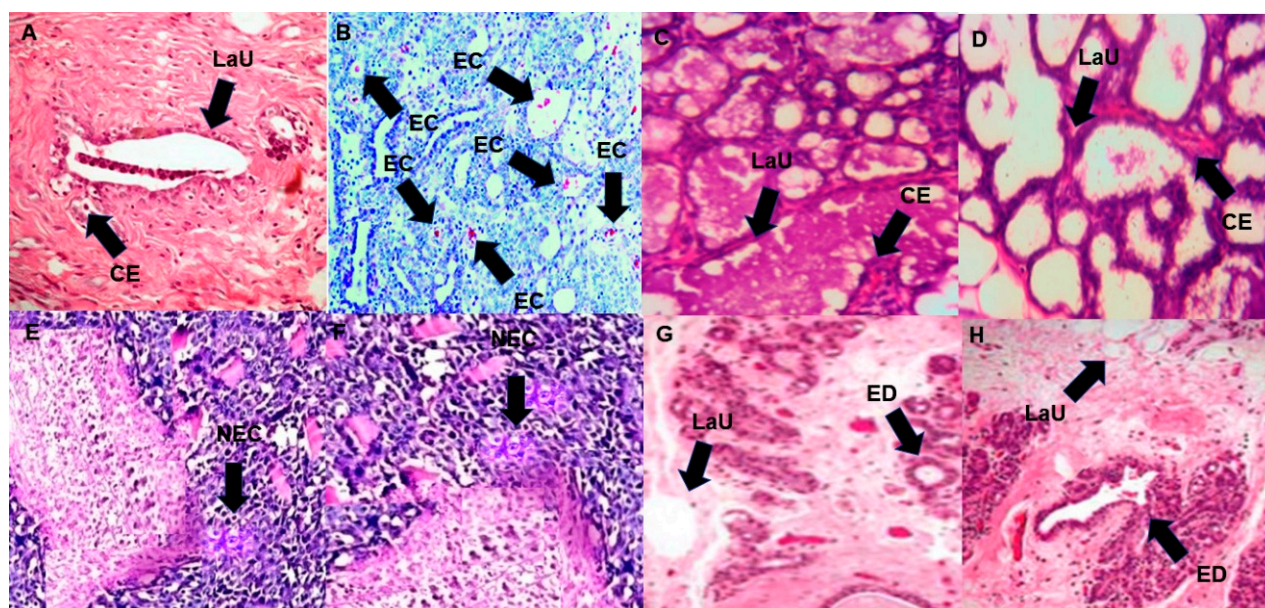


Figure 9. Photomicrograph of breast section of a normal control rat showing lobuloalveolar unit (LaU) and cuboidal epithelial cells (CE) (A); photomicrograph of breast section treated with MNU showing mammary gland carcinoma alongside with massive proliferation of neoplastic epithelial cells (EC) (B); photomicrograph of breast section treated with 3DPQ-12 in a concentration of 5 mg/kg

of bwt showing lobuloalveolar unit (LaU) and cuboidal epithelial cells (CE) (C); photomicrograph of breast section treated with **3DPQ-12** in concentration of 50 mg/kg of bwt showing lobuloalveolar unit (LaU) and cuboidal epithelial cells (CE) (D); photomicrograph of breast section treated with **4-OHT** in a concentration of 5 mg/kg of bwt showing necrosis (NEC) (E); photomicrograph of breast section treated with **4-OHT** in concentration of 50 mg/kg of bwt showing necrosis (NEC) (F); photomicrograph of breast section treated with **Ral** in a concentration of 5 mg/kg of bwt showing differentiated extralobular ducts (ED) (G); photomicrograph of breast section treated with **Ral** in a concentration of 50 mg/kg of bwt showing differentiated extralobular ducts (ED) (H), shown in $\times 200$ magnification and stained with hematoxylin and eosin.

Finally, the compounds were assayed for the maximum tolerated dose (MTD) or maximum feasible dose (MFD, in the absence of MTD) and weight loss (WL) studies (Table 11). Compounds and controls were daily re-administered per os in five doses, 5, 50, 100, 500, and 1000 mg/kg bwt [160] for 5 days. On the 5th day, the body weights were measured, and the postmortem evaluations were performed by means of a gross examination of all the animals at the terminal necropsy, as well as the histopathological examination of lungs, spleen, liver, kidneys, heart, and colon (Supplementary Materials Figures S219–S224, respectively). Hence, except for **MNU**, with an MTT of 100 mg/kg bwt, no mortality was observed in the treatment groups for 5 days even at the highest dose (Table 11). The orally administered compounds **3DPQ-12**, **3DPQ-3**, **3DPQ-9**, **3DPQ-4**, **3DPQ-2**, and **3DPQ-1** did not produce significant changes in body weight. Moreover, no obvious pathologic changes were observed based on histology or necropsy compared to placebo-treated controls. Therefore, given that the Food and Drug Administration (FDA) recommends 1000 mg/kg bwt as the high limit dose for acute, subchronic, and chronic toxicity studies in rodents and non-rodents [160], MTDs were not explicitly determined, and the 1000 mg/kg bwt could be considered as MFD (<https://www.fda.gov/drugs/guidance-compliance-regulatory-information/guidances-drugs>, accessed on 1 March 2022) for **3DPQ-12**, **3DPQ-3**, **3DPQ-9**, **3DPQ-4**, **3DPQ-2**, and **3DPQ-1** [160]. All the compounds were proven safe for further pre-clinical and clinical trials at a concentration of 50 mg/kg bwt.

3. Materials and Methods

3.1. ER α LBD-Partial Agonists/Antagonists Complexes Structures Preparation

The 39 complexes of ER α partial agonists and antagonists, co-crystallized with either wild-type (WT) or mutated (MUT) receptors, retrieved from PDB (TR, Table 1: 18 WT ER α binders with the activities reported as pIC₅₀s; Table 2: 8 MUT ER α binders with the activities reported as pIC₅₀s) and test set (TS_{CRY}, Table 3: 13 WT and MUT ER α binders with the activities reported as pK_is) were prepared [93,161] using the validated procedures described elsewhere [80,92] (see the Supplementary Materials: Crystal structures compilation and preparation and Supporting Information Table S1 for detailed information).

3.2. 3-D Pharmacophore Hypotheses and 3-D QSAR Models Generation

A set of 3-D pharmacophore hypotheses and atom-based 3-D QSAR models were generated using the PHASE software [88] as implemented in Schrödinger's suite [89], using the default setup (see the Supplementary Materials: Pharmacophore modeling and 3-D QSAR modeling for detailed information). For the statistically best hypotheses/models (endowed with the highest q^2 values), robustness was confirmed by means of leave-one-out (LOO) and leave-some-out (LSO) cross-validations (CV) [80,92] while lack of chance correlation was checked by a Y-scrambling procedure [80,92]. Models were graphically interpreted by means of UCSF Chimera [93].

3.3. SB Alignment Assessment

All the scoring functions of the Glide software [104–106], as implemented in Schrödinger's Suite [89], were evaluated to select the best one to perform an SB alignment assessment

on TR compounds. The SB procedure was assessed through four methods, similar to those previously described in [80,92]: experimental conformation re-docking (ECDR), randomized conformation re-docking (RCRD), experimental conformation cross-docking (ECCD), and randomized conformation cross-docking (RCCD). The experimental protocols and Glide's settings [105,106] are reported in the Supplementary Materials: Alignment assessment rules, Ligand's experimental conformations randomizations, and Glide settings.

3.4. LB Alignment Assessment

To rule out the LB molecular alignment of TR compounds, all the available scoring functions of the flexible ligand alignment tool (FLA) [89], as implemented in Schrödinger's Suite [89], were evaluated. The LB alignment procedure assessment was conducted at different levels of difficulty, similar to those previously described in [80,92]: experimental conformation re-alignment (ECRA), randomized conformation re-alignment (RCRA), experimental conformation cross-alignment (ECCA), and randomized conformation cross-alignment (RCCA). The experimental protocols and FLA setup [89] are reported in the sections Supplementary Materials: Alignment assessment rules and Flexible Ligand Alignment tool settings.

3.5. The SB/LB Alignment Accuracy

The alignment fitness was then quantified by evaluating both the RMSD and the subsequent docking accuracy (DA) and alignment accuracy (AA), as previously reported [80,92]. Both DA and AA were used to evaluate how the algorithms used could predict the ligand poses as closely as possible to the experimentally observed ones, by separating the correctly ($\text{RMSD} \leq 2 \text{ \AA}$) and partially ($2 \text{ \AA} \leq \text{RMSD} \leq 3 \text{ \AA}$) docked/aligned poses for those mis-docked/mis-aligned ($\text{RMSD} \geq 3 \text{ \AA}$). The rules for DA and AA calculation are reported in Supplementary Materials *Alignment assessment rules* section.

3.6. Generation of Modeled and Designed Compounds

Either TS_{MOD1} 's, TS_{MOD2} 's, and TS_{MOD3} 's (Supplementary Materials Tables S10–S15) or the designed compounds (Table 8) were drawn through the Chemaxon's msketch module [103] by means of the optimization of the molecular mechanics using the MMFF94 force field and the default settings, upon which the hydrogen atoms were assigned at pH 7.4. Upon structures' generation, compounds were uploaded into previously described best-performing SB and LB protocols to obtain the bioactive conformations (see Supplementary Materials: Alignment assessment rules, Structure-based alignment assessments, and Ligand-based alignment assessments).

3.7. Test Sets and Designed Compounds Alignment

The TS_{MOD1} , TS_{MOD2} , and TS_{MOD3} (Supplementary Materials Tables S10–S15), as well as all the designed compounds (Table 6), were aligned applying either the best performing SB or LB protocols (see Supplementary Materials: Test sets alignment, Alignment assessment rules, Structure-based alignment assessments, and Ligand-based alignment assessments).

3.8. Virtual Screening

The virtual screening of NCI compound libraries (486 compounds from Natural Products Set 3 and 1574 and 2351 compounds from the Diversity Sets 2 and 3), taken from the NCI (NCI, <https://www.cancer.gov/>, accessed on 1 October 2015) was conducted following the guidelines as described elsewhere [90,91]. The compounds were retrieved in structure data file (sdf) format, split into individual files, imported in Chemaxon's msketch module [103], and energy minimized by means of molecular mechanics' optimization using the MMFF94 force field and the default settings, upon which the hydrogen atoms were assigned at pH 7.4. Upon the generation of the structures, compounds were uploaded into previously determined best-performing SB and LB protocols to perform

cross-docking and cross-alignment and obtain the bioactive conformations against ER α (see Supplementary Materials: Virtual screening, Alignment assessment rules, Structure-based alignment assessments, and Ligand-based alignment assessments).

3.9. 3-D Pharmacophore Hypotheses and 3-D QSAR Models External Validation and Prediction Ability

The TS_{CRY} (Table 5), TS_{MOD1}, TS_{MOD2}, TS_{MOD3} (Supporting Information Tables S10–S15), virtually screened compounds (Supporting Information Tables S16–S17), and the designed compounds (Table 6) were imported into the best **3-D pharmacophore hypothesis/3-D QSAR model** ensemble (see 3-D pharmacophore and 3-D QSAR modeling and models' interpretation) and predicted by means of the activity [80,92].

3.10. Synthesis of Compounds 3DPQ-1 to 3DPQ-12

All the experimental work regarding the conventional synthesis of designed compounds **3DPQ-1** to **3DPQ-12**, as well as regarding spectral data interpretation and purity, is described in detail as Supplementary Materials under the Experimental and Results and discussion sections, respectively.

3.11. ADMETox Predictions for Compounds 3DPQ-1 to 3DPQ-12

The ADMETox properties were predicted by means of Schrödinger's QikProp module [144] and admetSAR 2.0 webserver (<http://lmmd.ecust.edu.cn/admetSar2>, accessed on 1 March 2022) [145], using the default setup.

3.12. Biochemical Evaluation

All the biochemical experimental work was performed following the guidelines already reported in the literature. These are detailed in Supporting Materials, under the Experimental sections: Synthesized Compounds Antagonistic Potency and Relative Binding Affinities to ER α and ER β [128,129], Synthesized Compounds Antiproliferative Activity against ER α (+)- and ER α (-)-Dependent Breast Cancer Cell Lines [130], ER α Down-Regulation [138,139], ER α Functional Antagonism Cell Assay [15,74,131], The Impact of targeted ER α Antagonists on the MCF-7 Cells Signaling [132–135], Effects of Synthesized Compounds on Cytotoxicity and Cell Cycle Distribution in ER α (+)Dependent Breast Cancer Cell Lines [130], Determination of Lipophilicity [74,156], In vivo Anticancer Screening [146], Measurement of Serum Biochemical Markers [159], Determination of Antioxidant Markers in Liver Homogenate [159], Plasma Protein Binding Determination [139], Determination of the Intrinsic Clearance of Hepatocytes [158], Pharmacokinetics Studies In Rats [158], and Histopathological Studies [159].

4. Conclusions

The reported investigation summarizes the usage of rational drug design protocol by means of the SB and LB techniques to disclose new potent and selective antagonists against ER α as in vitro and in vivo anticancer agents, which emerged upon the lead optimization of the virtually screened compound Brefeldin A. The SB 3-D pharmacophore/QSAR models, coupled with molecular docking and ligand-based alignment, were revealed to be effective tools in the design of new Brefeldin A derivatives and were used for the very first time to describe their potency against ER α in physiological conditions, using the ER α antagonists and partial agonists co-crystallized within both wild-type or mutated receptors. Notably, the models emerged from a wide-ranging molecular diversity within the training set, consisting of a variety of antagonists and partial agonists associated with SERDs, SERMs, and naturally occurring sub-groups of compounds. The best **ADDHHHP.13** hypothesis (**3-DPhypI**), alongside the derived 3-D QSAR model, differentiated full antagonists from partial agonists and provided some guidelines for the selectivity toward ER α , describing all the important 3-D pharmacophoric properties desired for a powerful SERM to occupy the natural hormonal environment and to invoke in perspective the complete shut-down

of estrogen-initiated basal transcriptional machinery. Moreover, the **ADDHHHP.13** hypothesis was used to virtually screen NCI datasets disclosing BFA as an interesting hit, which was structurally optimized by engineering twelve innovative SERMs, **3DPQ-1** to **3DPQ-12**, that were synthesized, and broadly biochemically evaluated as ER α antagonists, as prospective BC suppressants. From determining the antagonistic potential against ER α , to elaborating the antiproliferative activity in ER α (+) BC cell lines, including the impact on the inner mechanisms of cancer development and toxicity predicted *in silico*, all of the designed and synthesized hits exerted notable potency, where slight differences in the activity can be understood from the structure-based point of view. The *in vivo* administration to adult Wistar rats discriminated the lead compounds by means of their impact on mammary tumorigenesis. Hence, **3DPQ-12**, **3DPQ-3**, **3DPQ-9**, **3DPQ-4**, **3DPQ-2**, and **3DPQ-1** were indeed found to be as potent as Ral, the most potent compound listed in the TR, at any stage of evaluation. By exerting more-than-promising anticancer activity, a favorable preclinical profile, and notable safety, **3DPQ-12**, **3DPQ-3**, **3DPQ-9**, **3DPQ-4**, **3DPQ-2**, and **3DPQ-1** can be considered candidates for pre-clinical and clinical trials as the future of SERM-related BC clinical therapy. In a future study, a model for the ER β antagonists will be also developed to design selective antagonists.

Supplementary Materials: The following are available online at <https://www.mdpi.com/article/10.3390/molecules27092823/s1>. This material contains the Introduction (i.e., The Genomic classical pathway, Genomic indirect pathway, Tethered pathway alternative routes, Non-genomic pathways, Abbreviations, ER α 3-D pharmacophore models generation overview), Results and discussion (i.e., Tables and Figures describing data sets compilation, 3-D pharmacophore models, 3-D QSAR models, SB and LB alignment assessments, activity prediction of test sets, virtual screening, designed compounds SB and LB alignments, synthesized compounds spectral data interpretation, Figures of ^1H NMR, ^{13}C NMR, ^{15}N NMR, ^{17}O NMR, and HPLC spectral data of synthesized precursors and bioactive compounds, related tables with biochemical data), and Experimental section (i.e., the training set selection, preparation of antagonists-ER α complexes, interpretation of 3-D QSARs, SB and LB alignment assessment rules definition, virtual screening, equipment, commercial compounds supply, synthetic protocols, the *in vitro* and *in vivo* experimental protocols). Figure S1–S9: Data associated with the 3-D pharmacophore and 3-D QSAR model interpretation, Figures S10–S19: Data associated with the structure-based and ligand-based alignment assessments, Figures S20–S22: Data associated with the virtual screening, Figures S23–S25: Data associated with designed compounds binding conformations, Figures S26–S177: Data associated with synthesized compound ^1H NMR, ^{13}C NMR, ^{15}N NMR, ^{17}O NMR spectra, Figures S178–S190: Data associated with synthesized compound HPLC spectra, Figures S191–S224: Data associated with synthesized compound biological activity *in vitro* and *in vivo*, Tables S1–S6: Data associated with the 3-D pharmacophore and 3-D QSAR models development, Tables S7–S9: Data associated with the structure-based and ligand-based alignment assessments, Tables S10–S15: Data associated with the external validation of 3-D pharmacophore and 3-D QSAR models predictive abilities, Tables S16–S17: Data associated with the virtual screening, Table S18: Data associated with designed compounds binding conformations, Tables S19–S20: Data associated with the synthesized compounds' toxicity.

Author Contributions: Conceptualization, M.M. and R.R.; methodology, M.M. and R.R.; software, M.M.; validation N.K., N.T., S.M., E.P., M.S., L.A., M.M. and R.R.; formal analysis, M.M. and R.R.; investigation, N.K., N.T., S.M., E.P., M.S., L.A., M.M. and R.R.; resources, N.K., N.T., S.M., E.P., M.S., L.A., M.M. and R.R.; data curation, N.K., N.T., S.M., E.P., M.S., L.A., M.M. and R.R.; writing—original draft preparation, M.M. and R.R.; writing—review and editing, M.S., L.A., M.M. and R.R.; visualization, M.M. and R.R.; supervision, M.M. and R.R.; project administration, M.M. and R.R.; funding acquisition, M.M. and R.R. All authors have read and agreed to the published version of the manuscript.

Funding: This research was funded by the Serbian Ministry of Education, Science and Technological Development (Agreement No. 451-03-68/2022-14/200122 and Agreement No. 451-03-68/2022-14/200378) and supported by two grants from Progetti di Ricerca di Università 2015, Sapienza Università di Roma (C26A15RT82 and C26A15J3BB).

Institutional Review Board Statement: All the animal procedures were approved by the Committee for Ethical Animal Care and Use of the Institute for Biological Research, Belgrade, which acts according to the Guide for the Care and Use of Laboratory Animals, published by the US National Institute of Health (NIH Publication No. 85/23, revised in 1986). Additionally, the Approvals for conducting scientific research on experimental animals were given to S.M. and M.M. by the Ethical Committee, Faculty of Science, University of Kragujevac (2020/2021).

Informed Consent Statement: Not applicable.

Data Availability Statement: All the experimental complexes used to build the 3-D pharmacophore and 3-D QSAR models, as well as the structure-based and ligand-based alignment assessments, can be retrieved free of charge from Protein Data Bank (<https://www.rcsb.org/>, accessed on 1 October 2015). All the compound structures used as test sets can be found in the Protein Data Bank or retrieved from the cited literature (see Supplementary Materials for specifics). All the computational results from 3-D pharmacophore and 3-D QSAR models studies and structure-based/ligand-based alignment assessments, as well as the UCSF Chimera sessions, are available from Milan Mladenović (files in machine-readable formats, e-mail: milan.mladenovic@pmf.kg.ac.rs). All the computational results regarding the design of new compounds can be obtained from Rino Ragno (e-mail: rino.ragno@uniroma1.it) and Milan Mladenović. Datasets for virtual screening can be obtained from National Cancer Institute (<https://www.cancer.gov/>, accessed on 1 October 2015). Open Access Software. The UCSF Chimera software, used for graphical analysis of 3-D QSAR models and structure-based and ligand-based aligned structures can be obtained free of charge at <https://www.cgl.ucsf.edu/chimera/> (accessed on 1 October 2015). Marvin Beans for academics can be obtained free of charge at <http://www.chemaxon.com> (accessed on 1 October 2015). Commercial Software. Schrödinger Suite can be obtained from Canvas, Schrödinger, LLC, New York, NY. ChemDraw can be obtained from PerkinElmer Informatics (<http://www.cambridgesoft.com/>, accessed on 1 October 2015) and was herein used from drawing structures under the academic license bought by the University of Kragujevac, Faculty of Science, Milan Mladenović's home institution. The Office365 package can be obtained from Microsoft Office (<https://www.office.com/>, accessed on 1 January 2022) and was herein used for writing and preparing figures under the academic license bought by the University of Kragujevac, Faculty of Science, Milan Mladenović's home institution.

Conflicts of Interest: The authors declare no conflict of interest.

Sample Availability: Samples of the compounds 3DPQ-1 to 3DPQ-12 are available from the authors.

References

1. Bafna, D.; Ban, F.; Rennie, P.S.; Singh, K.; Cherkasov, A. Computer-Aided Ligand Discovery for Estrogen Receptor Alpha. *Int. J. Mol. Sci.* **2020**, *21*, 4193. [[CrossRef](#)] [[PubMed](#)]
2. Shiau, A.K.; Barstad, D.; Radek, J.T.; Meyers, M.; Nettles, K.W.; Katzenellenbogen, B.S.; Katzenellenbogen, J.A.; Agard, D.A.; Greene, G.L. Structural Characterization of a Subtype-Selective Ligand Reveals a Novel Mode of Estrogen Receptor Antagonism. *Nat. Genet.* **2002**, *9*, 359–364. [[CrossRef](#)] [[PubMed](#)]
3. Ng, H.W.; Perkins, R.; Tong, W.; Hong, H. Versatility or Promiscuity: The Estrogen Receptors, Control of Ligand Selectivity and an Update on Subtype Selective Ligands. *Int. J. Environ. Res. Public Health* **2014**, *11*, 8709–8742. [[CrossRef](#)] [[PubMed](#)]
4. Galluzzo, P.; Ascenzi, P. Estrogen Signaling Multiple Pathways to Impact Gene Transcription. *Curr. Genom.* **2006**, *7*, 497–508. [[CrossRef](#)]
5. Ali, S.; Coombes, R.C. Estrogen Receptor Alpha in Human Breast Cancer: Occurrence and Significance. *J. Mammary Gland Biol. Neoplasia* **2000**, *5*, 271–281. [[CrossRef](#)] [[PubMed](#)]
6. Marc, R.; Monique, G.; Wurtz, J.M.; Moras, D. Estrogen Receptor Transcription and Transactivation: Structure-Function Relationship in DNA- and Ligand-Binding Domains of Estrogen Receptors. *Breast Cancer Res.* **2000**, *2*, 353–359.
7. Farooq, A. Structural and Functional Diversity of Estrogen Receptor Ligands. *Curr. Top. Med. Chem.* **2015**, *15*, 1372–1384. [[CrossRef](#)]
8. Kumar, R.; Zakharov, M.N.; Khan, S.H.; Miki, R.; Jang, H.; Toraldo, G.; Singh, R.; Bhasin, S.; Jasuja, R. The Dynamic Structure of the Estrogen Receptor. *J. Amino Acids* **2011**, *2011*, 812540. [[CrossRef](#)]
9. Bentrem, D.; Dardes, R.; Liu, H.; MacGregor-Schafer, J.; Zapf, J.; Jordan, V. Molecular Mechanism of Action at Estrogen Receptor Alpha of a New Clinically Relevant Antiestrogen (GW7604) Related to Tamoxifen. *Endocrinology* **2001**, *142*, 838–846. [[CrossRef](#)]

10. Safe, S.; Kim, K. Non-Classical Genomic Estrogen Receptor (ER)/Specificity Protein and ER/Activating Protein-1 Signaling Pathways. *J. Mol. Endocrinol.* **2008**, *41*, 263–275. [[CrossRef](#)]
11. Heldring, N.; Pike, A.; Andersson, S.; Matthews, J.; Cheng, G.; Hartman, J.; Tujague, M.; Ström, A.; Treuter, E.; Warner, M.; et al. Estrogen Receptors: How Do They Signal and What Are Their Targets. *Physiol. Rev.* **2007**, *87*, 905–931. [[CrossRef](#)] [[PubMed](#)]
12. Schwabe, J.; Chapman, L.; Finch, J.T.; Rhodes, D. The Crystal Structure of the Estrogen Receptor DNA-Binding Domain Bound to DNA: How Receptors Discriminate between their Response Elements. *Cell* **1993**, *75*, 567–578. [[CrossRef](#)]
13. Brzozowski, A.M.; Pike, A.C.W.; Dauter, Z.; Hubbard, R.E.; Bonn, T.; Engström, O.; Öhman, L.; Greene, G.L.; Gustafsson, J.A.; Carlquist, M. Molecular Basis of Agonism and Antagonism in the Oestrogen Receptor. *Nature* **1997**, *389*, 753–758. [[CrossRef](#)] [[PubMed](#)]
14. Wardell, S.E.; Ellis, M.J.; Alley, H.M.; Eisele, K.; VanArsdale, T.; Dann, S.G.; Arndt, K.T.; Primeau, T.; Griffin, E.; Shao, J.; et al. Efficacy of SERD/SERM Hybrid-CDK4/6 Inhibitor Combinations in Models of Endocrine Therapy-Resistant Breast Cancer. *Clin. Cancer Res.* **2015**, *21*, 5121–5130. [[CrossRef](#)]
15. Patel, H.K.; Bihani, T. Selective Estrogen Receptor Modulators (SERMs) and Selective Estrogen Receptor Degradators (SERDs) in Cancer Treatment. *Pharmacol. Ther.* **2018**, *186*, 1–24. [[CrossRef](#)]
16. Maximov, P.Y.; Lee, T.M.; Jordan, V.C. The Discovery and Development of Selective Estrogen Receptor Modulators (SERMs) for Clinical Practice. *Curr. Clin. Pharmacol.* **2013**, *8*, 135–155. [[CrossRef](#)]
17. Lu, Y.; Liu, W. Selective Estrogen Receptor Degradators (SERDs): A Promising Strategy for Estrogen Receptor Positive Endocrine-Resistant Breast Cancer. *J. Med. Chem.* **2020**, *63*, 15094–15114. [[CrossRef](#)]
18. Bai, Z.; Gust, R. Breast Cancer, Estrogen Receptor and Ligands. *Arch. Pharm.* **2009**, *342*, 133–149. [[CrossRef](#)]
19. Dadiboyena, S. Recent Advances in the Synthesis of Raloxifene: A Selective Estrogen Receptor Modulator. *Eur. J. Med. Chem.* **2012**, *51*, 17–34. [[CrossRef](#)]
20. Begam, A.J.; Jubie, S.; Nanjan, M. Estrogen Receptor Agonists/Antagonists in Breast Cancer Therapy: A Critical Review. *Bioorganic Chem.* **2017**, *71*, 257–274. [[CrossRef](#)]
21. Fanning, S.W.; Mayne, C.G.; Dharmarajan, V.; Carlson, K.E.; Martin, T.A.; Novick, S.J.; Toy, W.; Green, B.; Panchamukhi, S.; Katzenellenbogen, B.S.; et al. Estrogen Receptor Alpha Somatic Mutations Y537S and D538G Confer Breast Cancer Endocrine Resistance by Stabilizing the Activating Function-2 Binding Conformation. *eLife* **2016**, *5*, e12792. [[CrossRef](#)] [[PubMed](#)]
22. Anstead, G.M.; Carlson, K.E.; Katzenellenbogen, J.A. The Estradiol Pharmacophore: Ligand Structure-Estrogen Receptor Binding Affinity Relationships and a Model for The Receptor Binding Site. *Steroids* **1997**, *62*, 268–303. [[CrossRef](#)]
23. Wolber, G.; Langer, T. LigandScout: 3-D Pharmacophores Derived from Protein-Bound Ligands and Their Use as Virtual Screening Filters. *J. Chem. Inf. Model.* **2005**, *45*, 160–169. [[CrossRef](#)]
24. Yusharyahya, S.N.; Bramono, K.; Ascobat, P.; Hestiantoro, A.; Sutanto, N.R.; Fadilah, F. In silico Molecular Docking and Pharmacophore Modelling Studies of *Trigonella foenum-graceum* (fenugreek) Interactions with Estrogen Receptors α and β . *J. Pharm. Sci. Res.* **2019**, *11*, 3705–3711.
25. McGregor, M.J.; Muskal, S.M. Pharmacophore Fingerprinting. 1. Application to QSAR and Focused Library Design. *J. Chem. Inf. Comput. Sci.* **1999**, *39*, 569–574. [[CrossRef](#)]
26. *Discovery Studio*; Accelrys Software Inc.: San Diego, CA, USA, 2007.
27. *Catalyst Software Package*; Accelrys Software Inc.: San Diego, CA, USA, 2007.
28. Mukherjee, S.; Nagar, S.; Mullick, S.; Mukherjee, A.; Saha, A. Pharmacophore Mapping of Selective Binding Affinity of Estrogen Modulators through Classical and Space Modeling Approaches: Exploration of Bridged-Cyclic Compounds with Diarylethylene Linkage. *J. Chem. Inf. Model.* **2007**, *47*, 475–487. [[CrossRef](#)] [[PubMed](#)]
29. Mukherjee, S.; Nagar, S.; Mullick, S.; Mukherjee, A.; Saha, A. Pharmacophore Mapping of Arylbenzothiophene Derivatives for MCF Cell Inhibition Using Classical and 3D Space Modeling Approaches. *J. Mol. Graph. Model.* **2008**, *26*, 884–892. [[CrossRef](#)] [[PubMed](#)]
30. Islam, M.A.; Nagar, S.; Das, S.; Mukherjee, A.; Saha, A. Molecular Design Based on Receptor-Independent Pharmacophore: Application to Estrogen Receptor Ligands. *Biol. Pharm. Bull.* **2008**, *31*, 1453–1460. [[CrossRef](#)] [[PubMed](#)]
31. Brogi, S.; Kladi, M.; Vagias, C.; Papazafiri, P.; Roussis, V.; Tafi, A. Pharmacophore Modeling for Qualitative Prediction of Antiestrogenic Activity. *J. Chem. Inf. Model.* **2009**, *49*, 2489–2497. [[CrossRef](#)] [[PubMed](#)]
32. Fang, J.; Shen, J.; Cheng, F.; Xu, Z.; Liu, G.; Tang, Y. Computational Insights into Ligand Selectivity of Estrogen Receptors from Pharmacophore Modeling. *Mol. Inf.* **2011**, *30*, 539–549. [[CrossRef](#)]
33. Brogi, S.; Papazafiri, P.; Roussis, V.; Tafi, A. 3D-QSAR using pharmacophore-based alignment and Virtual Screening for discovery of Novel MCF-7 Cell Line Inhibitors. *Eur. J. Med. Chem.* **2013**, *67*, 344–351. [[CrossRef](#)]
34. Muchtaridi, M.; Yusuf, M.; Diantini, A.; Choi, S.B.; Al-Najjar, B.O.; Manurung, J.V.; Subarnas, A.; Achmad, T.H.; Wardhani, S.R.; Wahab, H.A. Potential Activity of Fevicordin-A from *Phaleria macrocarpa* (Scheff) Boerl. Seeds as Estrogen Receptor Antagonist Based on Cytotoxicity and Molecular Modelling Studies. *Int. J. Mol. Sci.* **2014**, *15*, 7225–7249. [[CrossRef](#)] [[PubMed](#)]
35. Huang, W.; Wei, W.; Yang, Y.; Zhang, T.; Shen, Z. Discovery of Novel Selective ER α /ER β Ligands by Multi-pharmacophore Modeling and Virtual Screening. *Chem. Pharm. Bull.* **2015**, *63*, 780–791. [[CrossRef](#)] [[PubMed](#)]
36. Niinivehmas, S.P.; Manivannan, E.; Rauhamäki, S.; Huuskonen, J.; Pentikäinen, O.T. Identification of Estrogen Receptor Ligands with Virtual Screening Techniques. *J. Mol. Graph. Model.* **2016**, *64*, 30–39. [[CrossRef](#)] [[PubMed](#)]

37. Md Islam, A.; Patel, D.A.; Rathod, S.G.; Chunarkar, P.; Pillay, T.S. Identification of Structural Requirement of Estrogen Receptor Modulators using Pharmacoinformatics Techniques for Application to Estrogen Therapy. *Med. Chem. Res.* **2016**, *25*, 407–421. [[CrossRef](#)]
38. Chu, Z.; Li, Y. Designing Modified Polybrominated Diphenyl Ether BDE-47, BDE-99, BDE-100, BDE-183, and BDE-209 Molecules with Decreased Estrogenic Activities using 3D-QSAR, Pharmacophore Models Coupled with Resolution V of the 2^{10-3} Fractional Factorial Design and Molecular Docking. *J. Hazard. Mater.* **2019**, *364*, 151–162. [[CrossRef](#)]
39. Yu, E.; Xu, Y.; Shi, Y.; Yu, Q.; Liu, J.; Xu, L. Discovery of Novel Natural Compound Inhibitors Targeting Estrogen Receptor α by an Integrated Virtual Screening Strategy. *J. Mol. Model.* **2019**, *25*, 278–288. [[CrossRef](#)]
40. Scott, J.S.; Bailey, A.; Davies, R.D.; Degorce, S.L.; MacFaul, P.A.; Gingell, H.; Moss, T.; Norman, R.A.; Pink, J.H.; Rabow, A.A.; et al. Tetrahydroisoquinoline Phenols: Selective Estrogen Receptor Downregulator Antagonists with Oral Bioavailability in Rat. *ACS Med. Chem. Lett.* **2015**, *7*, 94–99. [[CrossRef](#)]
41. Tria, G.S.; Abrams, T.; Baird, J.; Burks, H.E.; Firestone, B.; Gaither, L.A.; Hamann, L.G.; He, G.; Kirby, C.A.; Kim, S.; et al. Discovery of LSZ102, a Potent, Orally Bioavailable Selective Estrogen Receptor Degradator (SERD) for the Treatment of Estrogen Receptor Positive Breast Cancer. *J. Med. Chem.* **2018**, *61*, 2837–2864. [[CrossRef](#)]
42. Mardianingrum, R.; Yusuf, M.; Hariono, M.; Gazzali, M.A.; Muchtaridi, M. α -Mangostin and its Derivatives against Estrogen Receptor Alpha. *J. Biomol. Struct. Dyn.* **2022**, *40*, 2621–2634. [[CrossRef](#)] [[PubMed](#)]
43. Hariyanti, H.; Kusmardi, K.; Yanuar, A.; Hayun, H. Ligand Based Pharmacophore Modeling, Virtual Screening, and Molecular Docking Studies of Asymmetrical Hexahydro-2H-Indazole Analogs of Curcumin (AIACs) to Discover Novel Estrogen Receptors Alpha (ER α) Inhibitor. *Indones. J. Chem.* **2021**, *21*, 137–147. [[CrossRef](#)]
44. Jereva, D.; Fratev, F.; Tsakovska, I.; Alov, P.; Pencheva, T.; Pajeva, I. Molecular Dynamics Simulation of the Human Estrogen Receptor Alpha: Contribution to the Pharmacophore of the Agonists. *Math. Comput. Simul.* **2017**, *133*, 124–134. [[CrossRef](#)]
45. Gangloff, M.; Ruff, M.; Eiler, S.; Duclaud, S.; Wurtz, J.M.; Moras, D. Crystal Structure of a Mutant hER α Ligand-Binding Domain Reveals Key Structural Features for the Mechanism of Partial Agonism. *J. Biol. Chem.* **2001**, *276*, 15059–15065. [[CrossRef](#)]
46. Nettles, K.W.; Bruning, J.B.; Gil, G.; O'Neill, E.E.; Nowak, J.; Guo, Y.; Kim, Y.; DeSombre, E.R.; Dilis, R.; Hanson, R.N.; et al. Structural Plasticity in the Oestrogen Receptor Ligand-Binding Domain. *EMBO Rep.* **2007**, *8*, 563–568. [[CrossRef](#)] [[PubMed](#)]
47. *Molecular Operating Environment (MOE)*, 2019.01; Chemical Computing Group ULC: Montreal, QC, Canada, 2017.
48. Munir, A.; Azam, S.; Mehmood, A.; Khan, Z.; Mehmood, A.; Fazal, S. Structure-Based Pharmacophore Modeling, Virtual Screening and Molecular docking for the Treatment of ESR1 Mutations in Breast Cancer. *Drug Des.* **2016**, *5*, 137–148. [[CrossRef](#)]
49. Heldring, N.; Pawson, T.; McDonnell, D.; Treuter, E.; Gustafsson, J.A.; Pike, A.C. Structural Insights into Corepressor Recognition by Antagonist-Bound Estrogen Receptors. *J. Biol. Chem.* **2007**, *282*, 10449–10455. [[CrossRef](#)]
50. Fanning, S.W.; Jeselsohn, R.; Dharmarajan, V.; Mayne, C.G.; Karimi, M.; Buchwalter, G.; Houtman, R.; Toy, W.; Fowler, C.E.; Han, R.; et al. The SERM/SERD Bazedoxifene Disrupts ESR1 Helix 12 to Overcome Acquired Hormone Resistance in Breast Cancer Cells. *Elife* **2018**, *7*, e37161. [[CrossRef](#)]
51. Muchtaridi, M.; Syahidah, H.N.; Subarnas, A.; Yusuf, M.; Bryant, S.D.; Langer, T. Molecular Docking and 3D-Pharmacophore Modeling to Study the Interactions of Chalcone Derivatives with Estrogen Receptor Alpha. *Pharmaceuticals* **2017**, *10*, 81. [[CrossRef](#)] [[PubMed](#)]
52. Muchtaridi, M.; Yusuf, M.; Syahidah, H.N.; Subarnas, A.; Zamri, A.; Bryant, S.D.; Langer, T. Cytotoxicity of Chalcone of *Eugenia aquae Burm F* Leaves Against T47D Breast Cancer Cell Lines and Its Prediction as An Estrogen Receptor Antagonist Based on Pharmacophore-Molecular Dynamics Simulation. *Adv Appl. Bioinform. Chem.* **2019**, *12*, 33–43. [[CrossRef](#)]
53. Sahayarayan, J.J.; Rajan, K.S.; Vidhyavathi, R.; Nachiappan, M.; Prabhu, D.; Alfarraj, S.; Arokiyaraj, S.; Daniel, A.N. In-silico Protein-Ligand Docking Studies against the Estrogen Protein of Breast Cancer Using Pharmacophore Based Virtual Screening Approaches. *Saudi J. Biol. Sci.* **2021**, *28*, 400–407. [[CrossRef](#)]
54. Shylaja, R.; Loganathan, C.; Kabilan, S.; Vijayakumar, T.; Meganathan, C. Synthesis and Evaluation of the Antagonistic Activity of 3-acetyl-2H-benzo[g]chromen-2-one against Mutant Y537S Estrogen Receptor Alpha via E-Pharmacophore Modeling, Molecular Docking, Molecular Dynamics, and in-vitro Cytotoxicity Studies. *J. Mol. Struct.* **2021**, *224*, 129289. [[CrossRef](#)]
55. Nwachukwu, J.C.; Srinivasan, S.; Zheng, Y.; Wang, S.; Min, J.; Dong, C.; Liao, Z.; Nowak, J.; Wright, N.J.; Houtman, R.; et al. Predictive Features of Ligand-Specific Signaling through the Estrogen Receptor. *Mol. Syst. Biol.* **2016**, *12*, 864. [[CrossRef](#)] [[PubMed](#)]
56. Nwachukwu, J.C.; Srinivasan, S.; Bruno, N.E.; Nowak, J.; Wright, N.J.; Minutolo, F.; Rangarajan, E.S.; Izard, T.; Yao, X.Q.; Grant, B.J.; et al. Systems Structural Biology Analysis of Ligand Effects on ER α Predicts Cellular Response to Environmental Estrogens and Anti-hormone Therapies. *Cell Chem. Biol.* **2017**, *24*, 35–45. [[CrossRef](#)]
57. Srinivasan, S.; Nwachukwu, J.C.; Bruno, N.E.; Dharmarajan, V.; Goswami, D.; Kastrati, I.; Novick, S.; Nowak, J.; Cavett, V.; Zhou, H.B.; et al. Full Antagonism of the Estrogen Receptor Without a Prototypical Ligand Side Chain. *Nat. Chem. Biol.* **2017**, *13*, 111–118. [[CrossRef](#)]
58. Speltz, T.E.; Fanning, S.W.; Mayne, C.G.; Fowler, C.; Tajkhorshid, E.; Greene, G.L.; Moore, T.W. Stapled Peptides with γ -Methylated Hydrocarbon Chains for the Estrogen Receptor/Coactivator Interaction. *Angew. Chem. Int. Ed. Engl.* **2016**, *55*, 4252–4555. [[CrossRef](#)]
59. Wu, Y.-L.; Yang, X.; Ren, Z.; McDonnell, D.P.; Norris, J.; Willson, T.M.; Greene, G.L. Structural Basis for an Unexpected Mode of SERM-Mediated ER Antagonism. *Mol. Cell* **2005**, *18*, 413–424. [[CrossRef](#)]

60. Wärnmark, A.; Treuter, E.; Gustafsson, J.A.; Hubbard, R.E.; Brzozowski, A.M.; Pike, A.C. Interaction of Transcriptional Intermediary Factor 2 Nuclear Receptor Box Peptides with the Coactivator Binding Site of Estrogen Receptor Alpha. *J. Biol. Chem.* **2002**, *277*, 21862–21868. [[CrossRef](#)]
61. Kim, S.; Wu, J.Y.; Birzin, E.T.; Frisch, K.; Chan, W.; Pai, L.Y.; Yang, Y.T.; Mosley, R.T.; Fitzgerald, P.M.D.; Sharma, N.; et al. Estrogen Receptor Ligands. II. Discovery of Benzoxathiins as Potent, Selective Estrogen Receptor α Modulators. *J. Med. Chem.* **2004**, *47*, 2171–2175. [[CrossRef](#)]
62. Manas, E.S.; Unwalla, R.J.; Xu, Z.B.; Malamas, M.S.; Miller, C.P.; Harris, H.A.; Hsiao, C.; Akopian, T.; Hum, W.-T.; Malakian, K.; et al. Structure-Based Design of Estrogen Receptor- β Selective Ligands. *J. Am. Chem. Soc.* **2004**, *126*, 15106–15119. [[CrossRef](#)]
63. Manas, E.S.; Xu, Z.B.; Unwalla, R.J.; Somers, W.S. Understanding the Selectivity of Genistein for Human Estrogen Receptor-Beta Using X-Ray Crystallography and Computational Methods. *Structure* **2004**, *12*, 2197–2207. [[CrossRef](#)]
64. Blizzard, T.A.; DiNinno, F.; Morgan, J.D.; Chen, H.Y.; Wu, J.Y.; Kim, S.; Chan, W.; Birzin, E.T.; Yang, Y.T.; Pai, L.-Y.; et al. Estrogen Receptor Ligands. Part 9: Dihydrobenzoxathiin SERAMs with Alkyl Substituted Pyrrolidine Side Chains and Linkers. *Bioorg. Med. Chem. Lett.* **2005**, *15*, 107–113. [[CrossRef](#)] [[PubMed](#)]
65. Renaud, J.; Bischoff, S.F.; Buhl, T.; Floersheim, P.; Fournier, B.; Geiser, M.; Halleux, C.; Kallen, J.; Keller, H.; Ramage, P. Selective Estrogen Receptor Modulators with Conformationally Restricted Side Chains. Synthesis and Structure-Activity Relationship of ER α -Selective Tetrahydroisoquinoline Ligands. *J. Med. Chem.* **2005**, *48*, 364–379. [[CrossRef](#)] [[PubMed](#)]
66. Tan, Q.; Blizzard, T.A.; Morgan, J.D.; Birzin, E.T.; Chan, W.; Yang, Y.T.; Pai, L.-Y.; Hayes, E.C.; DaSilva, C.A.; Warriar, S.; et al. Estrogen receptor ligands. Part 10: Chromanes: Old Scaffolds for New SERAMs. *Bioorg. Med. Chem. Lett.* **2005**, *15*, 1675–1681. [[CrossRef](#)] [[PubMed](#)]
67. Kong, E.H.; Heldring, N.; Gustafsson, J.; Treuter, E.; Hubbard, R.E.; Pike, A.C.W. Delineation of A Unique Protein–Protein Interaction Site on the Surface of the Estrogen Receptor. *Proc. Natl. Acad. Sci. USA* **2005**, *102*, 3593–3598. [[CrossRef](#)]
68. Dykstra, K.D.; Guo, L.; Birzin, E.T.; Chan, W.; Yang, Y.T.; Hayes, E.C.; DaSilva, C.A.; Pai, L.Y.; Mosley, R.T.; Kraker, B.; et al. Estrogen Receptor Ligands. Part 16: 2-Aryl Indoles as Highly Subtype Selective Ligands for ER α . *Bioorg. Med. Chem. Lett.* **2007**, *17*, 2322–2328. [[CrossRef](#)]
69. Shiau, A.K.; Barstad, D.; Loria, P.M.; Cheng, L.; Kushner, P.J.; Agard, D.A.; Greene, G.L. The Structural Basis of Estrogen Receptor/Coactivator Recognition and the Antagonism of This Interaction by Tamoxifen. *Cell* **1998**, *95*, 927–937. [[CrossRef](#)]
70. Renaud, J.; Bischoff, S.F.; Buhl, T.; Floersheim, P.; Fournier, B.; Halleux, C.; Kallen, J.; Keller, H.; Schlaeppli, J.M.; Stark, W. Estrogen Receptor Modulators: Identification and Structure-Activity Relationships of Potent ER α -Selective Tetrahydroisoquinoline Ligands. *J. Med. Chem.* **2003**, *46*, 2945–2957. [[CrossRef](#)]
71. Hsieh, R.W.; Rajan, S.S.; Sharma, S.K.; Greene, G.L. Molecular Characterization of a B-ring Unsaturated Estrogen: Implications for Conjugated Equine Estrogen Components of Premarin. *Steroids* **2008**, *73*, 59–68. [[CrossRef](#)]
72. Nettles, K.W.; Bruning, J.B.; Gil, G.; Nowak, J.; Sharma, S.K.; Hahm, J.B.; Kulp, K.; Hochberg, R.B.; Zhou, H.; Katzenellenbogen, J.A.; et al. NF κ B Selectivity of Estrogen Receptor Ligands Revealed by Comparative Crystallographic Analyses. *Nat. Chem. Biol.* **2008**, *4*, 241–247. [[CrossRef](#)]
73. Dai, S.Y.; Chalmers, M.J.; Bruning, J.; Bramlett, K.S.; Osborne, H.E.; Montrose-Rafizadeh, C.; Barr, R.J.; Wang, Y.; Wang, M.; Burris, T.P.; et al. Prediction of the Tissue-Specificity of Selective Estrogen Receptor Modulators by Using a Single Biochemical Method. *Proc. Natl. Acad. Sci. USA* **2008**, *105*, 7171–7176. [[CrossRef](#)]
74. Degorce, S.L.; Bailey, A.; Callis, R.; De Savi, C.; Ducray, R.; Lamont, G.; MacFaul, P.; Maudet, M.; Martin, S.; Morgentin, R.; et al. Investigation of (E)-3-[4-(2-Oxo-3-aryl-chromen-4-yl)oxyphenyl]acrylic Acids as Oral Selective Estrogen Receptor Down-Regulators. *J. Med. Chem.* **2015**, *58*, 3522–3533. [[CrossRef](#)] [[PubMed](#)]
75. Delfosse, V.; Grimaldi, M.; Pons, J.-L.; Boulahtouf, A.; le Maire, A.; Cavailles, V.; Labesse, G.; Bourguet, W.; Balaguer, P. Structural and mechanistic insights into bisphenols action provide guidelines for risk assessment and discovery of bisphenol A substitutes. *Proc. Natl. Acad. Sci. USA* **2012**, *109*, 14930–14935. [[CrossRef](#)] [[PubMed](#)]
76. Osz, J.; Brélivet, Y.; Peluso-Iltis, C.; Cura, V.; Eiler, S.; Ruff, M.; Bourguet, W.; Rochel, N.; Moras, D. Structural basis for a molecular allosteric control mechanism of cofactor binding to nuclear receptors. *Proc. Natl. Acad. Sci. USA* **2012**, *109*, E588–E594. [[CrossRef](#)] [[PubMed](#)]
77. Delfosse, V.; Grimaldi, M.; Cavailles, V.; Balaguer, P.; Bourguet, W. Structural and Functional Profiling of Environmental Ligands for Estrogen Receptors. *Environ. Health Perspect.* **2014**, *122*, 1306–1313. [[CrossRef](#)]
78. Delfosse, V.; le Maire, A.; Balaguer, P.; Bourguet, W. A Structural Perspective on Nuclear Receptors as Targets of Environmental Compounds. *Acta Pharmacol. Sin.* **2014**, *36*, 88–101. [[CrossRef](#)]
79. Zheng, Y.; Zhu, M.; Srinivasan, S.; Nwachukwu, J.; Cavett, V.; Min, J.; Carlson, K.E.; Wang, P.; Dong, C.; Katzenellenbogen, J.A.; et al. Development of Selective Estrogen Receptor Modulator (SERM)-Like Activity Through an Indirect Mechanism of Estrogen Receptor Antagonism: Defining the Binding Mode of 7-Oxabicyclo [2.2.1]hept-5-ene Scaffold Core Ligands. *ChemMedChem* **2012**, *7*, 1094–1100. [[CrossRef](#)]
80. Mihović, N.; Tomašević, N.; Matić, S.; Mitrović, M.M.; Kostić, D.A.; Sabatino, M.; Antonini, L.; Ragno, R.; Mladenović, M. Human Estrogen Receptor α Antagonists. Part 1: 3-D QSAR-Driven Rational Design of Innovative Coumarin-Related Antiestrogens as Breast Cancer Suppressants through Structure-Based and Ligand-Based Studies. *J. Chem. Inf. Model.* **2021**, *61*, 5028–5053. [[CrossRef](#)]

81. Kurtanović, N.; Tomašević, N.; Matić, S.; Mitrović, M.M.; Kostić, D.A.; Sabatino, M.; Antonini, L.; Ragno, R.; Mladenović, M. Human Estrogen Receptor α Antagonists, part 2: Synthesis Driven by Rational Design, in vitro Antiproliferative, and in vivo Anticancer Evaluation of Innovative Coumarin-Related Antiestrogens as Breast Cancer Suppressants. *Eur. J. Med. Chem.* **2022**, *227*, 113869. [CrossRef]
82. Tanenbaum, D.M.; Wang, Y.; Williams, S.P.; Sigler, P.B. Crystallographic Comparison of the Estrogen and Progesterone Receptor's Ligand Binding Domains. *Proc. Natl. Acad. Sci. USA* **1998**, *95*, 5998–6003. [CrossRef]
83. Eiler, S.; Gangloff, M.; Duclaud, S.; Moras, D.; Ruff, M. Overexpression, Purification, and Crystal Structure of Native ER Alpha LBD. *Protein Expr. Purif.* **2001**, *22*, 165–173. [CrossRef]
84. Fang, J.; Akwabi-Ameyaw, A.; Britton, J.E.; Katamreddy, S.R.; Navas, F.; Miller, A.B.; Williams, S.P.; Gray, D.W.; Orband-Miller, L.A.; Shearin, J.; et al. Synthesis of 3-alkyl Naphthalenes as Novel Estrogen Receptor Ligands. *Bioorg. Med. Chem. Lett.* **2008**, *18*, 5075–5077. [CrossRef] [PubMed]
85. Srinivasan, S.; Nwachukwu, J.C.; Parent, A.A.; Cavett, V.; Nowak, J.; Hughes, T.S.; Kojetin, D.J.; Katzenellenbogen, J.A.; Nettles, K.W. Ligand-Binding Dynamics Rewire Cellular Signaling via Estrogen Receptor- α . *Nat. Chem. Biol.* **2013**, *9*, 326–332. [CrossRef] [PubMed]
86. Nwachukwu, J.C.; Srinivasan, S.; Bruno, N.E.; Parent, A.A.; Hughes, T.S.; Pollock, J.A.; Gjyshi, O.; Cavett, V.; Nowak, J.; Garcia-Ordonez, R.D.; et al. Resveratrol Modulates the Inflammatory Response via an Estrogen Receptor-Signal Integration Network. *Elife* **2014**, *3*, e02057. [CrossRef] [PubMed]
87. De Savi, C.; Bradbury, R.H.; Rabow, A.A.; Norman, R.A.; de Almeida, C.; Andrews, D.M.; Ballard, P.; Buttar, D.; Callis, R.J.; Currie, G.S.; et al. Optimization of a Novel Binding Motif to (E)-3-(3,5-difluoro-4-((1R,3R)-2-(2-fluoro-2-methylpropyl)-3-methyl-2,3,4,9-tetrahydro-1H-pyrido[3,4-b]indol-1-yl)phenyl)acrylic Acid (AZD9496), a Potent and Orally Bioavailable Selective Estrogen Receptor Downregulator and Antagonist. *J. Med. Chem.* **2015**, *58*, 8128–8140. [CrossRef]
88. Dixon, S.L.; Smondyrev, A.M.; Knoll, E.H.; Rao, S.N.; Shaw, D.E.; Friesner, R.A. PHASE: A new engine for pharmacophore perception, 3D QSAR model development, and 3D database screening: 1. Methodology and preliminary results. *J. Comput. Mol. Des.* **2006**, *20*, 647–671. [CrossRef]
89. *Schrödinger Release 2015-2: Canvas*; Schrödinger, LLC: New York, NY, USA, 2015.
90. Ballante, F.; Caroli, A.; Wickersham, R.B., 3rd; Ragno, R. Hsp90 Inhibitors, Part 1: Definition of 3-D QSAutogrid/R Models as a Tool for Virtual Screening. *J. Chem. Inf. Model.* **2014**, *54*, 956–969. [CrossRef]
91. Caroli, A.; Ballante, F.; Wickersham, R.B., 3rd; Corelli, F.; Ragno, R. Hsp90 Inhibitors, Part 2: Combining Ligand-Based and Structure-Based Approaches for Virtual Screening Application. *J. Chem. Inf. Model.* **2014**, *54*, 970–977. [CrossRef]
92. Mladenović, M.; Patsilnakos, A.; Pirolli, A.; Sabatino, M.; Ragno, R. Understanding the Molecular Determinant of Reversible Human Monoamine Oxidase B Inhibitors Containing 2H-Chromen-2-One Core: Structure-Based and Ligand-Based Derived Three-Dimensional Quantitative Structure–Activity Relationships Predictive Models. *J. Chem. Inf. Model.* **2017**, *57*, 787–814. [CrossRef]
93. Pettersen, E.F.; Goddard, T.D.; Huang, C.C.; Couch, G.S.; Greenblatt, D.M.; Meng, E.C.; Ferrin, T.E. UCSF Chimera—A visualization system for exploratory research and analysis. *J. Comput. Chem.* **2004**, *25*, 1605–1612. [CrossRef]
94. Fanning, S.W.; Hodges-Gallagher, L.; Myles, D.C.; Sun, R.; Fowler, C.E.; Plant, I.N.; Green, B.D.; Harmon, C.L.; Greene, G.L.; Kushner, P.J. Specific Stereochemistry of OP-1074 Disrupts Estrogen Receptor Alpha Helix 12 and Confers Pure Antiestrogenic Activity. *Nat. Commun.* **2018**, *9*, 2368–2379. [CrossRef]
95. Brozik, P.; Kocbek, P.; Sova, M.; Kristl, J.; Martens, S.; Adamski, J.; Gobec, S.; Lanisnik, R.T. Flavonoids and Cinnamic Acid Derivatives as Inhibitors of 17 β -Hydroxysteroid Dehydrogenase Type 1. *Mol. Cell. Endocrinol.* **2009**, *301*, 229–234. [CrossRef] [PubMed]
96. Rathelot, P.; Azas, N.; El-Kashef, H.; Delmas, F.; Di Giorgio, C.; Timon-David, P.; Maldonado, J.; Vanelle, P. 1,3-Diphenylpyrazoles: Synthesis and Antiparasitic Activities of Azomethine Derivatives. *Eur. J. Med. Chem.* **2002**, *37*, 671–679. [CrossRef]
97. Sun, J.; Huang, Y.R.; Harrington, W.R.; Sheng, S.; Katzenellenbogen, J.A.; Katzenellenbogen, B.S. Antagonists Selective for Estrogen Receptor Alpha. *Endocrinology* **2002**, *143*, 941–947. [CrossRef] [PubMed]
98. Rodriguez, A.L.; Tamrazi, A.; Collins, M.L.; Katzenellenbogen, J.A. Design, Synthesis, and in Vitro Biological Evaluation of Small Molecule Inhibitors of Estrogen Receptor Alpha Coactivator Binding. *J. Med. Chem.* **2004**, *47*, 600–611. [CrossRef] [PubMed]
99. Küçüköğlü, K.; Seçinti, H.; Özgür, A.; Seçen, H.; Tutar, Y. Synthesis, Molecular Docking, and Antitumoral Activity of Alnustone-Likecompounds Against Estrogen Receptor Alpha-Positive Human Breast Cancer. *Turk. J. Chem.* **2015**, *39*, 179–193. [CrossRef]
100. Yang, W.; Yong, W.; AiQian, Z.; HongXia, Y.; LianSheng, W. Three-Dimensional Quantitative Structure-Activity Relationships of Flavonoids and Estrogen Receptors Based on Docking. *Chin. Sci. Bull.* **2010**, *55*, 1488–1494. [CrossRef]
101. Stauffer, S.R.; Huang, Y.R.; Aron, Z.D.; Coletta, C.J.; Sun, J.; Katzenellenbogen, B.S.; Katzenellenbogen, J.A. Triarylpyrazoles with Basic Side Chains: Development of Pyrazole-Based Estrogen Receptor Antagonists. *Bioorg. Med. Chem.* **2001**, *9*, 151–161. [CrossRef]
102. Brian, E.F.; Deborah, S.M.; Shaun, R.S.; Zachary, D.A.; John, A.K. Novel Structural Templates for Estrogen-Receptor Ligands and Prospects for Combinatorial Synthesis of Estrogens. *Chem. Biol.* **1999**, *6*, 205–219. [CrossRef]
103. Marvin Beans 15.4.27.0, 2015, ChemAxon. Available online: <http://www.chemaxon.com> (accessed on 1 January 2015).
104. Herynk, M.H.; Fuqua, S.A.W. Estrogen Receptor Mutations in Human Disease. *Endocr. Rev.* **2004**, *25*, 869–898. [CrossRef] [PubMed]

105. Friesner, R.A.; Banks, J.L.; Murphy, R.B.; Halgren, T.A.; Klicic, J.J.; Mainz, D.T.; Repasky, M.P.; Knoll, E.H.; Shelley, M.; Perry, J.K.; et al. Glide: A New Approach for Rapid, Accurate Docking and Scoring. 1. Method and Assessment of Docking Accuracy. *J. Med. Chem.* **2004**, *47*, 1739–1749. [[CrossRef](#)]
106. Halgren, T.A.; Murphy, R.B.; Friesner, R.A.; Beard, H.S.; Frye, L.L.; Pollard, W.T.; Banks, J.L. Glide: A New Approach for Rapid, Accurate Docking and Scoring. 2. Enrichment Factors in Database Screening. *J. Med. Chem.* **2004**, *47*, 1750–1759. [[CrossRef](#)] [[PubMed](#)]
107. Friesner, R.A.; Murphy, R.B.; Repasky, M.P.; Frye, L.L.; Greenwood, J.R.; Halgren, T.A.; Sanschagrin, P.C.; Mainz, D.T. Extra Precision Glide: Docking and Scoring Incorporating a Model of Hydrophobic Enclosure for Protein–Ligand Complexes. *J. Med. Chem.* **2006**, *49*, 6177–6196. [[CrossRef](#)]
108. Tropsha, A. Best Practices for QSAR Model Development, Validation, and Exploitation. *Mol. Inform.* **2010**, *29*, 476–488. [[CrossRef](#)] [[PubMed](#)]
109. Ragno, R. www.3d-qsar.com: A Web Portal that Brings 3-D QSAR to all Electronic Devices-The Py-Comfa Web Application as Tool to Build Models from Pre-Aligned Datasets. *J. Comput. Aided. Mol. Des.* **2019**, *33*, 855–864. [[CrossRef](#)]
110. Ragno, R.; Esposito, V.; Di Mario, M.; Masiello, S.; Viscovo, M.; Cramer, R.D. Teaching and Learning Computational Drug Design: Student Investigations of 3D Quantitative Structure–Activity Relationships through Web Applications. *J. Chem. Educ.* **2020**, *97*, 1922–1930. [[CrossRef](#)] [[PubMed](#)]
111. Paek, S.-M. Recent Synthesis and Discovery of Brefeldin A Analogs. *Mar. Drugs* **2018**, *16*, 133. [[CrossRef](#)]
112. Lippincott-Schwartz, J.; Yuan, L.C.; Bonifacino, J.S.; Klausner, R.D. Rapid redistribution of Golgi proteins into the ER in cells treated with brefeldin A: Evidence for membrane cycling from Golgi to ER. *Cell* **1989**, *56*, 801–813. [[CrossRef](#)]
113. Dinter, A.; Berger, E.G. Golgi-disturbing agents. *Histochem. Cell Biol.* **1998**, *109*, 571–590. [[CrossRef](#)] [[PubMed](#)]
114. Seehafer, K.; Rominger, F.; Helmchen, G.; Langhans, M.; Robinson, D.G.; Özata, B.; Brügger, B.; Strating, J.R.P.M.; Van Kuppeveld, F.J.M.; Klein, C.D. Synthesis and Biological Properties of Novel Brefeldin A Analogues. *J. Med. Chem.* **2013**, *56*, 5872–5884. [[CrossRef](#)] [[PubMed](#)]
115. Anadu, N.O.; Davison, V.J.; Cushman, M. Synthesis and Anticancer Activity of Brefeldin A Ester Derivatives. *J. Med. Chem.* **2006**, *49*, 3897–3905. [[CrossRef](#)]
116. Argade, A.B.; Haugwitz, R.D.; Devraj, R.; Kozlowski, J.; Fanwick, A.P.E.; Cushman, M. Highly Efficient Diastereoselective Michael Addition of Various Thiols to (+)-Brefeldin A. *J. Org. Chem.* **1998**, *63*, 273–278. [[CrossRef](#)]
117. Kozikowski, A.P.; Shum, P.W.; Basu, A.; Lazo, J.S. Synthesis of Structural Analogues of Lyngbyatoxin A and Their Evaluation as Activators of Protein Kinase C. *J. Med. Chem.* **1991**, *34*, 2420–2430. [[CrossRef](#)]
118. Maki, B.E.; Scheidt, K.A. *N*-Heterocyclic Carbene-Catalyzed Oxidation of Unactivated Aldehydes to Esters. *Org. Lett.* **2008**, *10*, 4331–4334. [[CrossRef](#)] [[PubMed](#)]
119. Blakemore, P.R.; Kocienski, P.J.; Marzcek, S.; Wicha, J. The Modified Julia Olefination in Vitamin D₂ Synthesis. *Synthesis* **1999**, *1999*, 1209–1215. [[CrossRef](#)]
120. Förster, S.; Persch, E.; Tverskoy, O.; Rominger, F.; Helmchen, G.; Klein, C.; Gönen, B.; Brügger, B. Syntheses and Biological Properties of Brefeldin Analogues. *Eur. J. Org. Chem.* **2010**, *2011*, 878–891. [[CrossRef](#)]
121. Haynes, R.K.; Lam, W.W.-L.; Yeung, L.-L.; Williams, I.D.; Ridley, A.C.; Starling, S.M.; Vonwiller, S.C.; Hambley, T.W.; Lelandais, P. Highly Diastereoselective Conjugate Addition of Lithiated γ -Crotonolactone (But-2-en-4-olide) to Cyclic Enones to Give Syn-Adducts: Application to a Brefeldin Synthesis. *J. Org. Chem.* **1997**, *62*, 4552–4553. [[CrossRef](#)]
122. Trost, B.M.; Crawley, M.L. A “Chiral Aldehyde” Equivalent as a Building Block Towards Biologically Active Targets. *Chem. Eur. J.* **2004**, *10*, 2237–2252. [[CrossRef](#)]
123. Inanaga, J.; Hirata, K.; Saeki, H.; Katsuki, T.; Yamaguchi, M. A Rapid Esterification by Means of Mixed Anhydride and Its Application to Large-ring Lactonization. *Bull. Chem. Soc. Jpn.* **1979**, *52*, 1989–1993. [[CrossRef](#)]
124. Williams, D.R.; Jass, P.A.; Tse, H.L.A.; Gaston, R.D. Total synthesis of (+)-brenolide. *J. Am. Chem. Soc.* **1990**, *112*, 4552–4554. [[CrossRef](#)]
125. He, B.; Wang, Y.; Zheng, Y.; Chen, W.; Zhu, Q. Synthesis and Cytotoxic Evaluation of Acylated Brefeldin A Derivatives as Potential Anticancer Agents. *Chem. Biol. Drug Des.* **2013**, *82*, 307–316. [[CrossRef](#)] [[PubMed](#)]
126. Affini, A.; Hagenow, S.; Zivkovic, A.; Marco-Contelles, J.; Stark, H. Novel Indanone Derivatives as MAO B/H3R Dual-Targeting Ligands for Treatment of Parkinson’s Disease. *Eur. J. Med. Chem.* **2018**, *148*, 487–497. [[CrossRef](#)] [[PubMed](#)]
127. Yang, L.; Hu, Z.; Luo, J.; Tang, C.; Zhang, S.; Ning, W.; Dong, C.; Huang, J.; Liu, X.; Zhou, H.-B. Dual Functional Small Molecule Fluorescent Probes for Image-Guided Estrogen Receptor-Specific Targeting Coupled Potent Antiproliferative Potency For Breast Cancer Therapy. *Bioorganic Med. Chem.* **2017**, *25*, 3531–3539. [[CrossRef](#)]
128. Li, X.; Wu, C.; Lin, X.; Cai, X.; Liu, L.; Luo, G.; You, Q.; Xiang, H. Synthesis and Biological Evaluation of 3-Aryl-quinolin Derivatives as Anti-Breast Cancer Agents Targeting ER α and VEGFR-2. *Eur. J. Med. Chem.* **2018**, *161*, 445–455. [[CrossRef](#)] [[PubMed](#)]
129. Zhou, H.-B.; Sheng, S.; Compton, D.R.; Kim, Y.; Joachimiak, A.; Sharma, S.; Carlson, K.E.; Katzenellenbogen, B.S.; Nettles, K.W.; Greene, G.L.; et al. Structure-Guided Optimization of Estrogen Receptor Binding Affinity and Antagonist Potency of Pyrazolopyrimidines with Basic Side Chains. *J. Med. Chem.* **2006**, *50*, 399–403. [[CrossRef](#)]

130. Luo, G.; Li, X.; Zhang, G.; Wu, C.; Tang, Z.; Liu, L.; You, Q.; Xiang, H. Novel SERMs Based On 3-Aryl-4-Aryloxy-2H-Chromen-2-One Skeleton—A Possible Way to Dual ER α /VEGFR-2 Ligands for Treatment of Breast Cancer. *Eur. J. Med. Chem.* **2017**, *140*, 252–273. [[CrossRef](#)]
131. Callis, R.; Rabow, A.; Tonge, M.; Bradbury, R.; Challinor, M.; Roberts, K.; Jones, K.; Walker, G. A Screening Assay Cascade to Identify and Characterize Novel Selective Estrogen Receptor Downregulators (SERDs). *SLAS Discov. Adv. Sci. Drug Discov.* **2015**, *20*, 748–759. [[CrossRef](#)]
132. Lin, W.C.; Chuang, Y.C.; Chang, Y.S.; Lai, M.D.; Teng, Y.N.; Su, I.J.; Wang, C.C.; Lee, K.H.; Hung, J.H. Endoplasmic Reticulum Stress Stimulates p53 Expression Through NF- κ B Activation. *PLoS ONE* **2012**, *7*, e39120. [[CrossRef](#)]
133. Konduri, S.D.; Medisetty, R.; Liu, W.; Kaiparettu, B.A.; Srivastava, P.; Brauch, H.; Fritz, P.; Swetzig, W.M.; Gardner, A.E.; Khan, S.A.; et al. Mechanisms of Estrogen Receptor Antagonism toward p53 and its Implications in Breast Cancer Therapeutic Response and Stem Cell Regulation. *Proc. Natl. Acad. Sci. USA* **2010**, *107*, 15081–15086. [[CrossRef](#)]
134. Perissi, V.; Jepsen, K.; Glass, C.K.; Rosenfeld, M.G. Deconstructing repression: Evolving models of co-repressor action. *Nat. Rev. Genet.* **2010**, *11*, 109–123. [[CrossRef](#)]
135. Yang, X.J.; Seto, E. The Rpd3/Hda1 Family of Lysine Deacetylases: From Bacteria and Yeast to Mice and Men. *Nat. Rev. Mol. Cell Biol.* **2008**, *9*, 206–218. [[CrossRef](#)]
136. Dalvai, M.; Bystricky, K. Cell Cycle and Anti-Estrogen Effects Synergize to Regulate Cell Proliferation and ER Target Gene Expression. *PLoS ONE* **2010**, *5*, e11011. [[CrossRef](#)] [[PubMed](#)]
137. Elekofehinti, O.O.; Iwaloye, O.; Josiah, S.S.; Lawal, A.O.; Akinjiyan, M.O.; Ariyo, E.O. Molecular Docking Studies, Molecular Dynamics and ADME/Tox Reveal Therapeutic Potentials of STOCK1N-69160 against Papain-Like Protease of SARS-CoV-2. *Mol. Divers.* **2021**, *25*, 1761–1773. [[CrossRef](#)] [[PubMed](#)]
138. Lipinski, C.A.; Lombardo, F.; Dominy, B.W.; Feeney, P.J. Experimental and computational approaches to estimate solubility and permeability in drug discovery and development settings. *Adv. Drug Deliv. Rev.* **2001**, *46*, 3–26. [[CrossRef](#)] [[PubMed](#)]
139. Zhang, M.Q.; Wilkinson, B. Drug Discovery Beyond the ‘Rule-Of Five’. *Curr. Opin. Biotechnol.* **2007**, *18*, 478–488. [[CrossRef](#)]
140. Sun, H.; Li, Y.; Shen, M.; Tian, S.; Xu, L.; Pan, P.; Guan, Y.; Hou, T. Assessing the performance of MM/PBSA and MM/GBSA methods. 5. Improved docking performance using high solute dielectric constant MM/GBSA and MM/PBSA rescoring. *Phys. Chem. Chem. Phys.* **2014**, *16*, 22035–22045. [[CrossRef](#)]
141. Veber, D.F.; Johnson, S.R.; Cheng, H.-Y.; Smith, B.R.; Ward, K.W.; Kopple, K.D. Molecular Properties That Influence the Oral Bioavailability of Drug Candidates. *J. Med. Chem.* **2002**, *45*, 2615–2623. [[CrossRef](#)]
142. Congreve, M.; Carr, R.; Murray, C.; Jhoti, H. A Rule of Three for Fragment-Based Lead Discovery? *Drug Discov. Today* **2003**, *8*, 876–877. [[CrossRef](#)]
143. Köster, H.; Craan, T.; Brass, S.; Herhaus, C.; Zentgraf, M.; Neumann, L.; Heine, A.; Klebe, G. A Small Nonrule of 3 Compatible Fragment Library Provides High Hit Rate of Endothiapepsin Crystal Structures with Various Fragment Chemotypes. *J. Med. Chem.* **2011**, *54*, 7784–7796. [[CrossRef](#)]
144. *Schrödinger Release 2015-2: QikProp*; Schrödinger, LLC: New York, NY, USA, 2015.
145. Yang, H.; Lou, C.; Sun, L.; Li, J.; Cai, Y.; Wang, Z.; Li, W.; Liu, G.; Tang, Y. AdmetSAR 2.0: Web-service for prediction and optimization of chemical ADMET properties. *Bioinformatics* **2018**, *35*, 1067–1069. [[CrossRef](#)]
146. Mokale, S.N.; Begum, A.; Sakle, N.; Shelke, V.R.; Bhavale, S.A. Design, synthesis and anticancer screening of 3-(3-(substituted phenyl) acryloyl)-2H-chromen-2ones as selective anti-breast cancer agent. *Biomed. Pharmacother.* **2017**, *89*, 966–972. [[CrossRef](#)]
147. Quick, A.J.; Stanley-Brown, M.; Bancroft, F.W. A Study of the Coagulation Defect in Hemophilia and in Jaundice. *Am. J. Med. Sci.* **1935**, *190*, 501. [[CrossRef](#)]
148. Bergmeyer, H.U.; Bowers, G.N.; Hørder, M.; Moss, D.W. Provisional Recommendations on IFCC Methods for the Measurement of Catalytic Concentrations of Enzymes. Part 2. IFCC Method for Aspartat Aminotransferase. *Clin. Chim. Acta* **1976**, *70*, 19–42. [[CrossRef](#)]
149. Bergmeyer, H.U.; Hørder, M. IFCC Methods for Measurement of Catalytic Concentrations of Enzymes. *Clin. Chim. Acta* **1980**, *105*, 147–172. [[CrossRef](#)]
150. Walters, M.I.; Gerarde, H.W. An Ultramicromethod for the Determination of Conjugated and Total Bilirubin in Serum or Plasma. *Microchem. J.* **1970**, *15*, 231–243. [[CrossRef](#)]
151. Jendrassik, L.; Gróf, P. Vereinfachte Photometrische Methoden zur Bestimmung des Blutbilirubins. *Biochem. Z.* **1938**, *297*, 82–89.
152. Ellman, G.L. Tissue Sulfhydryl Groups. *Arch. Biochem. Biophys.* **1959**, *82*, 70–77. [[CrossRef](#)]
153. Góth, L.A. Simple Method for Determination of Serum Catalase Activity and Revision of Reference Range. *Clin. Chim. Acta* **1991**, *196*, 143–152. [[CrossRef](#)]
154. Ohkawa, H.; Ohishi, N.; Yagi, K. Assay for Lipid Peroxides in Animal Tissues by Thiobarbituric Acid Reaction. *Anal. Biochem.* **1979**, *95*, 351–358. [[CrossRef](#)]
155. Lowry, O.H.; Rosebrough, N.L.; Farr, A.L.; Randall, R.I. Protein Measurement with Folin Phenol Reagent. *J. Biol. Chem.* **1951**, *193*, 265–275. [[CrossRef](#)]
156. Green, C.E.; Swezey, R.; Bakke, J.; Shinn, W.; Furimsky, A.; Bejugam, N.; Shankar, G.N.; Jong, L.; Kapetanovic, I.M. Improved oral bioavailability in rats of SR13668, a novel anti-cancer agent. *Cancer Chemother. Pharmacol.* **2010**, *67*, 995–1006. [[CrossRef](#)]

157. Buttar, D.; Colclough, N.; Gerhardt, S.; MacFaul, P.A.; Phillips, S.D.; Plowright, A.; Whittamore, P.; Tam, K.; Maskos, K.; Steinbacher, S.; et al. A Combined Spectroscopic and Crystallographic Approach to probing Drug–Human Serum Albumin Interactions. *Bioorg. Med. Chem.* **2010**, *18*, 7486–7496. [[CrossRef](#)] [[PubMed](#)]
158. Soars, M.G.; Grime, K.; Sproston, J.L.; Webborn, P.J.H.; Riley, R.J. Use of Hepatocytes to Assess the Contribution of Hepatic Uptake to Clearance in Vivo. *Drug Metab. Dispos.* **2007**, *35*, 859–865. [[CrossRef](#)] [[PubMed](#)]
159. Stanković, N.; Mladenović, M.; Matić, S.; Stanić, S.; Mihailović, M.; Mihailović, V.; Katanić, J.; Boroja, T.; Vuković, N.; Sukdolak, S. Serum Albumin Binding Analysis and Toxicological Screening of Novel Chroman-2,4-Diones as Oral Anticoagulants. *Chem. Interact.* **2015**, *227*, 18–31. [[CrossRef](#)] [[PubMed](#)]
160. Bhatt, H.D.; McClain, S.; Lee, H.-M.; Zimmerman, T.; Deng, J.; Johnson, F.; Gu, Y.; Golub, L.M. The Maximum-Tolerated Dose and Pharmacokinetics of a Novel Chemically Modified Curcumin in Rats. *J. Exp. Pharmacol.* **2022**, *14*, 73–85. [[CrossRef](#)]
161. Case, D.A.; Darden, T.A.; Cheatham, T.E., III; Simmerling, C.L.; Wang, J.; Duke, R.E.; Luo, R.; Walker, R.C.; Zhang, W.; Merz, K.M.; et al. *AMBER 12*; University of California: San Francisco, CA, USA, 2012.